eawag aquatic research

Empa

Deliverable 4

Summary of the 2nd year of monitoring:
Aquifer's response to the first heating cycle

ARTS
Aquifer Reaction to Thermal Storage

Assessment of the aquifers' reaction to
High-Temperature Borehole Thermal Energy Storage

Dübendorf, 15.7.2026

Commissioned by: Swiss Federal Office of Energy

Contractor: Department of Water Resources and Drinking Water, Eawag

Authors: Joaquín Jiménez-Martínez (Eawag and ETH Zurich); Andrés Velásquez-Parra (Eawag)

Collaboration: Mario Schirmer, Christian Moeck, Reto Britt, Rolf Kipfer, Matthias Brennwald, Michael Berg, Andreas Voegelin, Lenny Winkel, Numa Pfenninger, Chiara Sancassani, Olga Schubert, Kim Trottmann, Serina Robinson, Megan Lee, Florian Altermatt, Roman Alther, Giulia Zecchin, Sarah Daker, Matthias Sulzer, Robert Weber, Lawrence Och.

Support BFE: Florence Begue; Stefano Benato; Pierre Christe; Christian Minnig.

Content

1. Summary 3
2. Monitoring concept 4
3. Update on geological characterization of the project area 7
4. HT-BTES operation and monitoring 8
5. Monitoring of the regional groundwater flow dynamics 10
6. Permanent monitoring 12
6.1 Groundwater physical properties 12
6.2 Concentration of dissolved gases 14
7. Periodic monitoring 16
7.1 Groundwater chemistry 16
7.1.1 Top aquifer of low-terrace gravels and glacial-lake deposits 16
7.1.2 Upper freshwater molasse 17
7.2 Microbiology 20
7.3 Environmental DNA 21
8. Conclusions 23
References 24
Appendix 1: Photographic record of the material core extracted from the observation borehole 4 (OB4) 25
Appendix 2: Lithological column for the observation borehole 4 (OB4) 27
Appendix 3: Summary of the time series of the concentration of dissolved gases 28
Appendix 4: Summary of the groundwater chemistry analyses performed for the top aquifer of low-terrace gravels and glacial-lake deposits (EE1t, EE2t, EE3t, and EE4t). 31
Appendix 5: Summary of the groundwater chemistry analyses performed for the upper freshwater molasse (EE1b and EE2b). 37

1. Summary

This document presents the Deliverable 4 of the ARTS project, which summarizes the monitoring results obtained during the second project year. This corresponds to the period in which the first heat injection was performed. This report assesses the effects of the temperature changes induced in the subsurface on the aquifer based on the monitoring activities carried out between June 2025 and early June 2026. It builds on the information and data shared so far in the Deliverable 3 from July 2025 and in the 2nd interim report from October 2025. We refer the reader to both reports whenever necessary.

The summarized data sets include on one hand the permanent monitoring measurements, corresponding to both groundwater physical properties and the concentration of dissolved gases, and on the hand the periodic monitoring activities, which include the laboratory analyses for groundwater chemistry, microbiology, and environmental DNA. In addition, results from the monitoring of the regional groundwater flow conditions are also presented. These data sets are also compared to the baseline-year describing the undisturbed aquifer behavior, which was presented in the Deliverable 3.

Overall, the monitoring of the first heat injection revealed only minor effects on the subsurface. These effects concern mainly the groundwater in the upper freshwater molasse close to the facility, where an increase in the concentration of some of the measured trace metals (Fe and Mn) and in some elements, such as Ba and Ca, was measured during the summer and autumn months of 2025. These changes did not persist during the winter time. In addition, an increase in the concentration of dissolved methane at the same location has been registered since the start of the injection. These effects point to an enhanced activity of the bacterial community identified so far in the molasse, which is characterized by microbial species know for inducing dissimilatory metal reduction and for mediating methanogenesis through the degradation of organic matter. In contrast to these observations, the monitoring results for the top aquifer of low-terrace gravels and glacial-lake deposits have not shown any significant variations. This difference in the response of both geologies might be explained by both the far longer residence time of groundwater in the molasse in areas where temperature changes have occurred, and the dissipation of the heat plume in the top aquifer due to the larger groundwater flow in this geology. We will continue monitoring these changes during the third year of the project to conclude on their direct relationship with the measured temperature changes and on their temporal evolution.

This report presents first a short review of the monitoring concept to provide context for the results discussed. This is followed by an update of the geological description of the project area based on the lithological column obtained for the observation borehole 4, which was recently drilled downstream from the facility. We then summarize the time series of the regional groundwater flow, and we describe the heat injection cycle performed in the summer of 2025. This is followed by a description of the main physical groundwater properties based on our monitoring data. Time series of the laboratory results are summarized in the subsequent chapters. A discussion on the interplay between the different monitoring activities is presented in the conclusions section. Additionally, the time series of all measured quantities are compiled in the attached appendixes.

2. Monitoring concept

The monitoring concept was designed with the goal of being able to assess the effects of cyclic temperature changes induced by the operation of the facility on the subsurface. It was conceived to capture such effects at locations upstream, downstream, and in direct vicinity of the facility, and in each case, at the two main geological units identified in the area, i.e., the top aquifer of low-terrace gravels and glacial-lake deposits, found up to an average depth of 35 m, and the upper freshwater molasse formation. This results in a total of six monitoring locations distributed in four observation boreholes (OB), as depicted in the two geological cross sections presented in Figure 1. The six locations have been labelled as EE{X}{Y}, where {X} represent the corresponding observation borehole, i.e., 1, 2, 3, or 4, and where {Y} indicates the monitored geology, i.e., *t* for the top aquifer, and *b* for the upper freshwater molasse. This nomenclature is employed in the remaining of this document to refer to any measurements belonging to these locations. Note that OB4 was drilled in December 2025 and only added to our monitoring concept since February 2026. Section 0 presents a short update on the geological description of the project area based on the geological column obtained from this drilling.

In addition to these three observation boreholes, six piezometers have been installed. Four of them, identified as P001, P002, P003, and P004, were drilled in the surroundings of the project area to monitor the regional groundwater flow conditions. Two more were defined as additional monitoring piezometers in the downstream area of the project and are labelled as P005 and P006. Figure 2 shows a general plan view of the project area with the exact location of all boreholes and piezometers.

Table 1. Summary of the variables measured during the continuous monitoring activities carried out at the three observation boreholes.

Device	Variable	Units	Observations
Flowmeter	Pumping flow rate	L/min	Measured for control of pumping operations
Diver (CTD)	Water head pressure	bar	Measured depth: • 14 m (OB1) ,18 m (OB2 & OB3) and 20 m (OB4) in the top aquifer • 68 m (OB1 & OB2) in the upper freshwater molasse
	Electrical conductivity (EC)	mS/cm	
	Groundwater temperature	°C	
	Air pressure	bar	Measured at the surface
	Air temperature	°C	
MiniRUEDI	Concentration of dissolved CH_4, N_2, O_2, Ar-40, CO_2, He-40, and Kr-80	hPa, mol/L	From water extracted at a depth of: • 16 m (OB1), and 20 m (OB2 & OB3) in the top aquifer • 70 m (OB1 & OB2) in the upper freshwater molasse

All datasets summarized in this report belong to the period between June 10th 2025 and May to June 2026. The exact period is mentioned in each corresponding section. Both a continuous and a periodic monitoring have been performed at all sampling locations. The continuous monitoring includes the measurement in depth of groundwater physical properties, such as temperature and electrical conductivity, as well as the measurement of the concentration of dissolved gases in the extracted groundwater. Note that the latter was changed to periodic monitoring since January 1st 2026 to improve the reliability of the mass spectrometers installed

on site. Periodic monitoring activities consist mainly in the extraction and further laboratory analysis of groundwater samples for the characterization of groundwater chemistry, microbiology, and groundwater fauna. Table 1 to Table 3 summarize the variables included in every monitoring activity and provide details on their measurement/sampling.

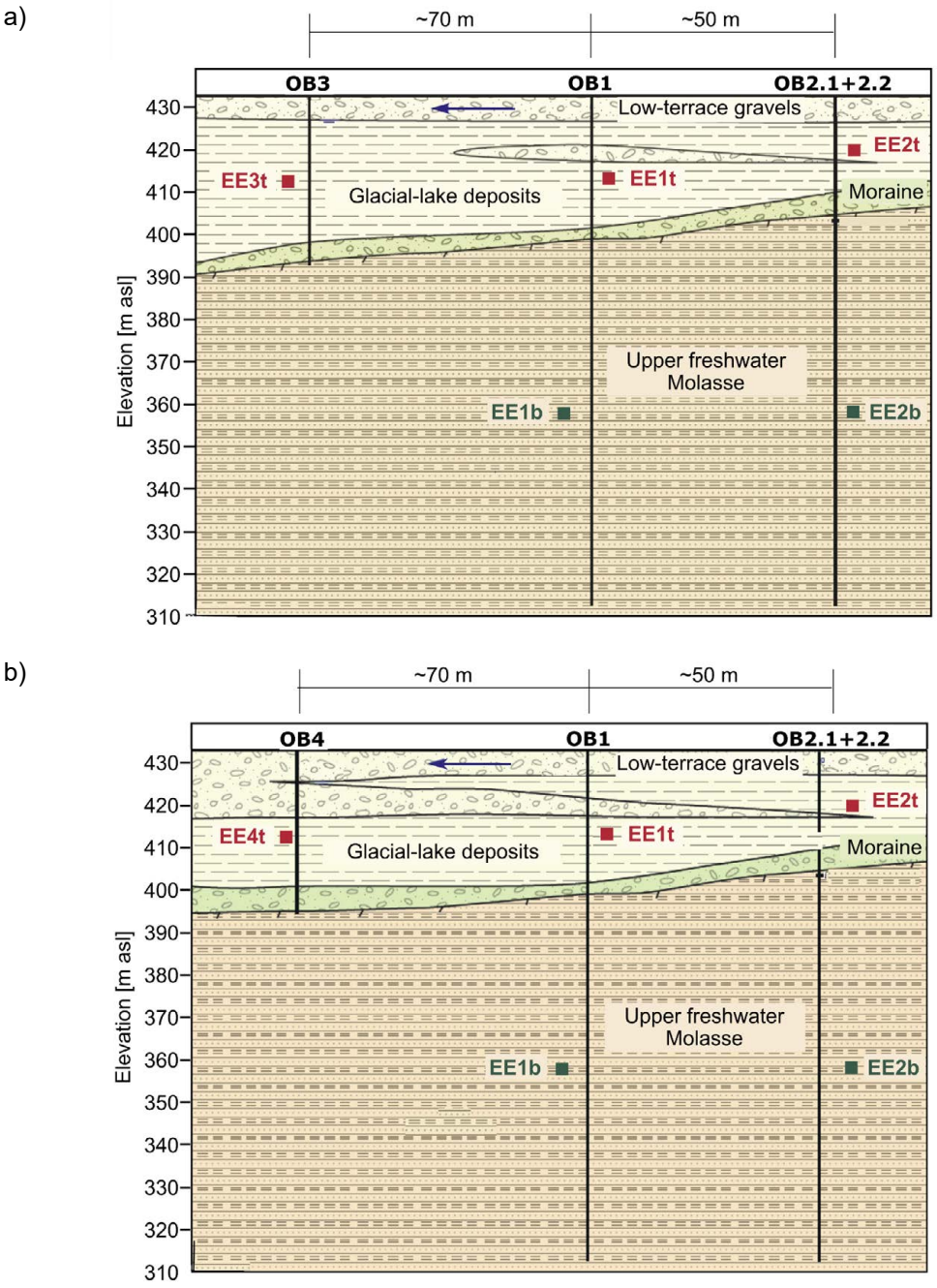

Figure 1. Geological profiles of the study site for the cross sections generated along a) observations boreholes1, 2 and 3 (OB1-OB2-OB3), and b) observation boreholes 1, 2, and 4 (OB1-OB2-OB4). The location of the corresponding OBs and of the resulting sampling locations, marked with the prefix EE, is indicated for each case.

Table 2. Summary of the variables measured continuously at the four surrounding piezometers employed to monitor the regional groundwater flow conditions.

Device	Variable	Units	Observations
Diver (CTD)	Water head pressure	bar	Measured depth: 5.60 m for P001, P002, P003, and P004
	Electrical conductivity (EC)	mS/cm	
	Groundwater temperature	°C	Measured depth: 5.60 m for P001, P002, P003, and P004 Second reading from the EC measurement available

Table 3. Summary of the variables analyzed through laboratory and field testing belonging to the periodic monitoring activities. They comprise analyses for the assessment of groundwater chemistry, microbiology, and groundwater fauna.

Activity	Variable	Units	Observations
Water Chemistry	pH*	-	From water extracted at a depth of: • 16 m (OB1), 20 m (OB2 & OB3) and 15 m (OB4) in the top aquifer • 70 m (OB1 & OB2) in the upper freshwater molasse *Also analyzed directly on site through field measurements
	Electrical conductivity (EC)*	µS/cm	
	Alkalinity	mmol/L	
	Hardness	mmol/L	
	Major ions concentrations: Br^-, Ca^{2+}, Cl^-, F^-, Mg^{2+}, K^+	mg/L	
	Nutrient concentrations: NH_4^+, NO^-_2, NO^-_3, PO_4^{3-}, SO_4^{2-}, total and dissolved phosphorous, total nitrogen	µg/L, mg/L	
	TOC, TIC	mg/L	
	Major and trace elements	µg/L	
	Dissolved oxygen concentration	mg/L, mbar, %	Directly measured on site on the extracted groundwater
	Redox potential	mV	
Microbiology	Population size (counted cells)	Events/µL	From groundwater sampled at a depth of: • 16 m (OB1), 20 m (OB2 & OB3) and 15 m (OB4) in the upper aquifer • 70 m (OB1 & OB2) in the upper freshwater molasse **Through filtration using Sterivex-filters. Relative abundance in collected samples.
	Bacterial community composition**	%	
Environmental DNA	DNA extract concentration	ng/µL	After filtering water extracted at a depth of: • 16 m (OB1), 20 m (OB2 & OB3) and 15 m (OB4) in the upper aquifer • 70 m (OB1 & OB2) in the freshwater molasse

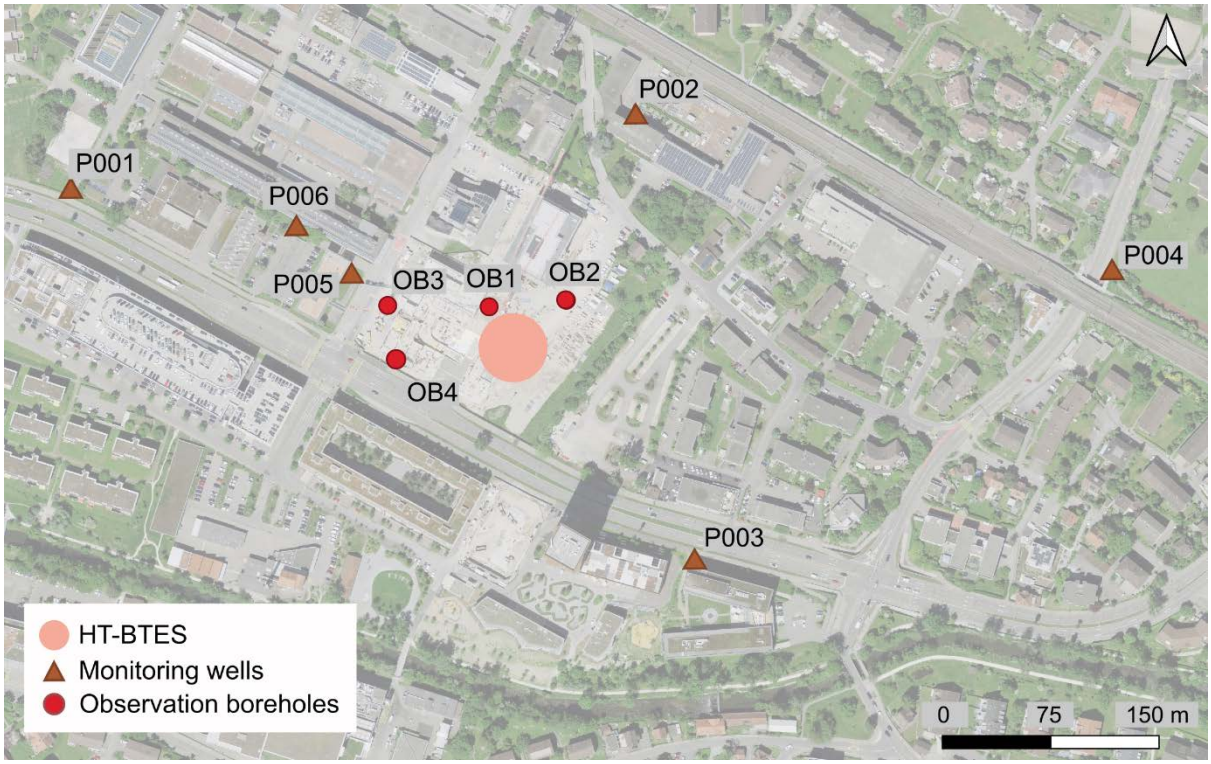

Figure 2. Plan view of the project area. The exact location of the HT-BTES facility, of the observation boreholes (OB) and of the additional piezometers (P) is displayed.

3. Update on geological characterization of the project area

The observation borehole 4 (OB4) was conceived as a second monitoring station in the downstream area, being located only 40 m south from OB3. Its design followed the same characteristics as OB3. Therefore, we kept the same diameter (4.5 inches) and the same screen design (filter tube starting at a depth of 6.0 m), until reaching the molasse rock. This occurred at a final depth of 38.0 m, in close agreement with the 39.0 m reached during the drilling of OB3.

The drilling of OB4 was carried out using a non-destructive wireline drilling/coring method. The extracted core was characterized on site, allowing for a detailed description of the geology at this location. This revealed important differences compared to the geology described so far at the other OBs. We identified a much thicker layer of the uppermost low-terrace gravels, reaching a total thickness of 15.6 m, far above the 6.0 m observed at OB1 and OB2 (see Figure 1b). As mentioned in several geological appraisals carried out in the past decades in the surrounding area, the layer of low-terrace gravels is responsible for most of the groundwater flow in the study site and can display hydraulic conductivities that can be up to two orders of magnitude larger than in the underlying glacial lake deposits. This thicker layer results in large contents of sand and medium-grained material at OB4, in contrast with the larger content of silt described at the other stations This more abundant coarser material can eventually lead to a larger groundwater flux towards the downstream area of the facility, promoting a fast movement of the heat plume in that direction. Figure 3 shows some impressions of the drilling work and of the obtained cores. Appendix 1 presents the entire core log, while Appendix 2 shows the complete lithological column at this location.

a) b)

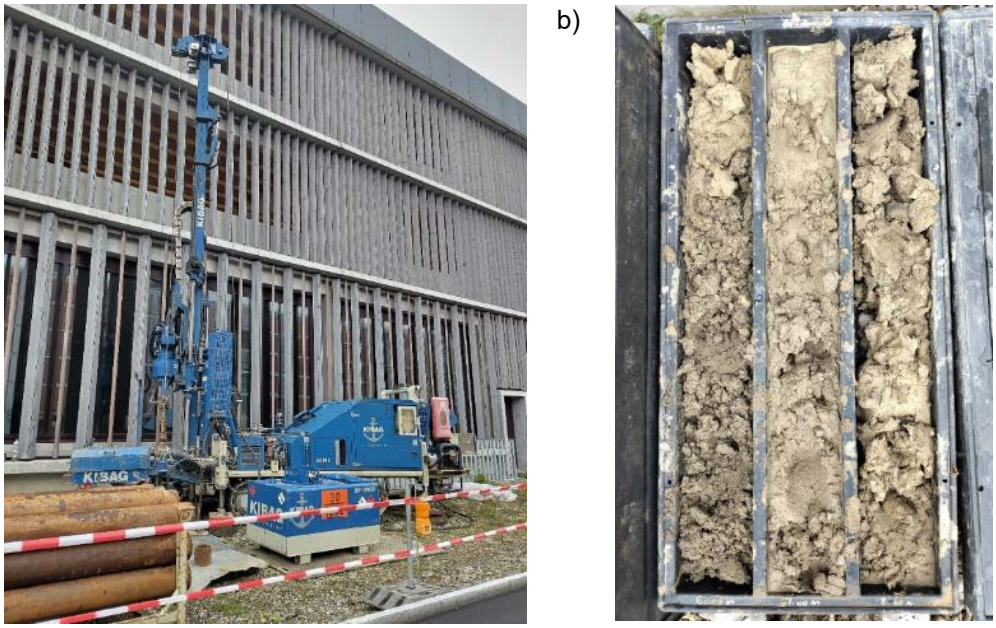

Figure 3. a) Impressions from the drilling of the observation borehole 4 (OB4). b) Example of the cores extracted from OB4 corresponding to the low-terrace gravels, for the stretch between 6.0 and 9.0 m depth.

4. HT-BTES operation and monitoring

The first heat injection took place during the second project year. Note that no injection took place in summer 2024. The heat injection officially started on June 11th 2025 and continued until September 21st 2025. During the initial phase, the BTES was only charged during normal working hours. This operating mode was chosen so that the BTES could be closely monitored, and any unforeseen events could be responded to quickly. From August 10th to September 9th, the system was switched to a 24-hours charging. After this prolonged heat injection phase, only short term injections occurred during the remainder of the monitoring year, namely in mid-November 2025, late January 2026, mid-February 2026, and more predominantly since April 2026. The continuous injection that has been taking place since the beginning of May 2026 will be considered as part of the second heat injection, which will be monitored during the third project year.

The heat was taken from the bidirectional medium-temperature network. In summer, this network serves as a waste heat network delivered by the campus chillers, whereas in winter it is used as a heating network for low-temperature heating systems. The temperatures on the warm side are regulated to 36-38°C and on the cold side to 28-30°C. By the end of 2025, around 720 MWh of heat were transferred to the BTES with inlet temperatures of about 30° to 38°C. Figure 4a shows the evolution of the heat and power injection over the observation time. The single periods of short-term injection over the fall and winter of 2025 are also displayed.

The temperatures induced inside the HT-BTES can be monitored using two fiber optic channels. They have been installed at target ground heat exchangers (GHE) to obtain temperature information at the eight injection rings that make up the facility. Figure 4b shows the location of these two channels together with all 144 GHEs. Each channel was installed parallel to the double-U tubing that distributes the water from one GHE to the next one. It provides temperature information at distances of 1.0 m, corresponding to a total measured length of approximately 1.5 km for each channel. Figure 5 shows the time evolution of the fiber optic temperature measurements over the entire 100 m-depth for the GHEs No. 7 and No.

128, which are located at the innermost and outermost ring, respectively. Results indicate maximum measured temperatures of 32.8 °C and 20.5 °C, respectively. This difference reflects the operation principle of a higher injection temperature in the inner rings compared to the outer ones.

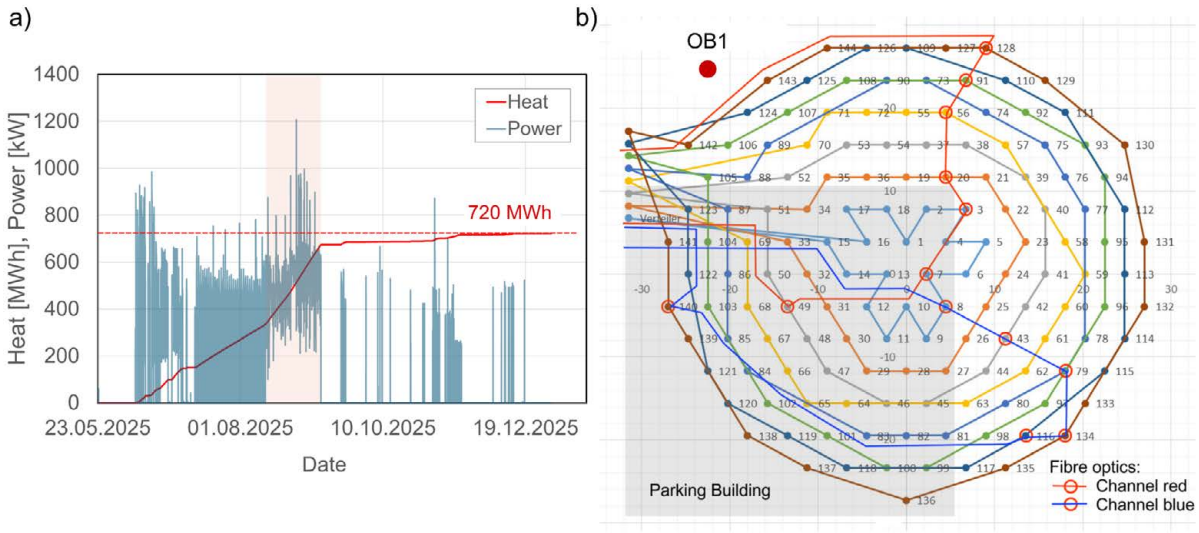

Figure 4. a) Time series of the =heat and power charged to the HT-BTES during the first heat injection cycle. The period of continuous heat injection is hatched red, and the cumulated heat flux by the end of 2025 is displayed. b) Plan view of the HT-BTES facility showing the location of the 144 ground heat exchangers (GHE) and their arrangement in eight different injection rings. The location of the two fiber optic channels used for temperature measurements over depth is also shown, as well as the location of the nearest observation borehole, OB1.

The effect of the two contrasting geological formations on heat storage is also visible. Figure 5a for the GHE No. 7 shows the dissipation of the temperature signal after the heat injection has been stopped. This dissipation occurs almost exclusively within the top aquifer (up to a depth of approximately 35 m) and is caused by the temperature and velocity of the incoming regional groundwater flow. This promotes the mixing of groundwater of different temperatures and the advection and dispersion of the heat plume in the downstream direction. In contrast, the temperature dissipation in the upper freshwater molasse during the winter months is far less pronounced, which agrees with the far lower flow velocities within that geology. A better glimpse at this effect can be obtained by generating a cross section of the HT-BTES facility in the West-East direction (approximate groundwater flow direction) using the temperature measurements of different GHEs belonging to both fiber optic channels. The plan view of the selected GHEs is shown in Figure 6, together with the temperature cross section at three different time steps covering the summer and winter time of 2025. The temperature maps were generated through linear interpolation of the temperature measurements of the selected GHEs over the length of the cross section. It can be observed that after the end of the peak injection period (Figure 6b), roughly three weeks are required to partially dissipate the temperature signal in the upper aquifer (Figure 6c). This condition resembles that observed during the winter period (Figure 6d), indicating that a permanent temperature change has been induced in both geologies. Please note that single short injection periods took place during autumn and likely contributed to the persistent temperature change in the subsurface. Overall, these observations indicate a fast transport and mixing mechanism responsible for the movement of the heat plume downstream from the HT-BTES facility.

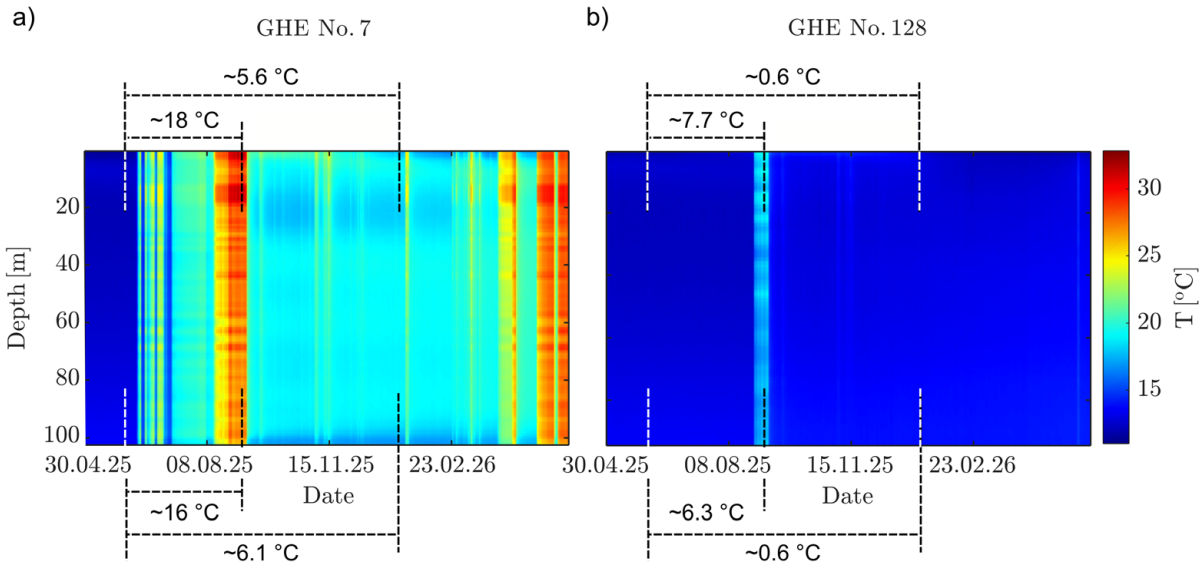

Figure 5. Temporal evolution of the temperature measurements registered at the fiber optic over depth for the ground heat exchangers (GHE) a) No. 7 (innermost ring) and b) No. 128 (outermost ring). The period between the end of April 2025 and end of May 2026 is displayed. The temperature scale is common to both subplots. The approximate temperature difference between the undisturbed condition (prior to the first injection) and both the peak injection time (end of August 2025) and the winter period (December 2025) is shown for the top aquifer and the freshwater molasse in the two subplots.

Figure 5a and Figure 5b also indicate the approximate temperature difference induced by the first heat injection cycle on both geologies compared to the condition prior to the injection for both the innermost and outermost ring of the facility, respectively. The induced temperature changes were similar for both geologies and were as large as 18 °C during the most intensive heat injection period (end of August 2025) and around 6.1 °C maximum during the winter months. Closer to our monitoring stations, namely at the outermost ring (GHE No. 128), temperature differences were far smaller, reaching a maximum of 7.7 °C by the end of August 2025 and only 0.6°C in the winter time. The fiber optic temperature measurements here presented offer valuable information to understand both the operation of the facility and the forcing that will control potential effects on the aquifer and the groundwater. The latter aspect is further discussed in the next sections, where the monitoring data is presented and contrasted with the above mentioned temperature changes.

5. Monitoring of the regional groundwater flow dynamics

The monitoring of the regional groundwater is based on the information of the piezometers P001, P002, P003 and P004, located in the areas surrounding the HT-BTES facility (see Figure 2). An overview of the variables continuously measured at these locations is presented in Table 2.

Figure 7 presents the time series of the groundwater table, h, calculated from the beginning of the records back in December 2024 until the end of April of 2026, using the pressure measurements collected at each station. Figure 7 also shows the time series of both the magnitude, ∇h, and direction, ∇h_{Dir}, of the groundwater gradient. Both were computed using a triangulation-based method, which employs the groundwater level information for different piezometer combinations (Devlin and Schillig, 2017; Moeck et al., 2018; Moeck et al., 2022). Note that the period between January 10th 2025 and February 17th 2025 was excluded from the analysis, since the groundwater table was being perturbed by pumping activities linked to

nearby excavation works. Overall, our results show no seasonality in the groundwater levels around the project area, and only minor variations in ∇h and ∇h_{Dir}, supporting the conclusion of constant regional groundwater flow conditions in the study site. From this analysis, we computed an average groundwater flow direction oriented at 194° (NE-SW) measured in counter-clockwise direction from a 0° degrees orientation pointing towards the east. Further details on the definition of the average groundwater flow direction can be found in Deliverable 3, as well as in the 2nd interim report submitted at the end of 2025.

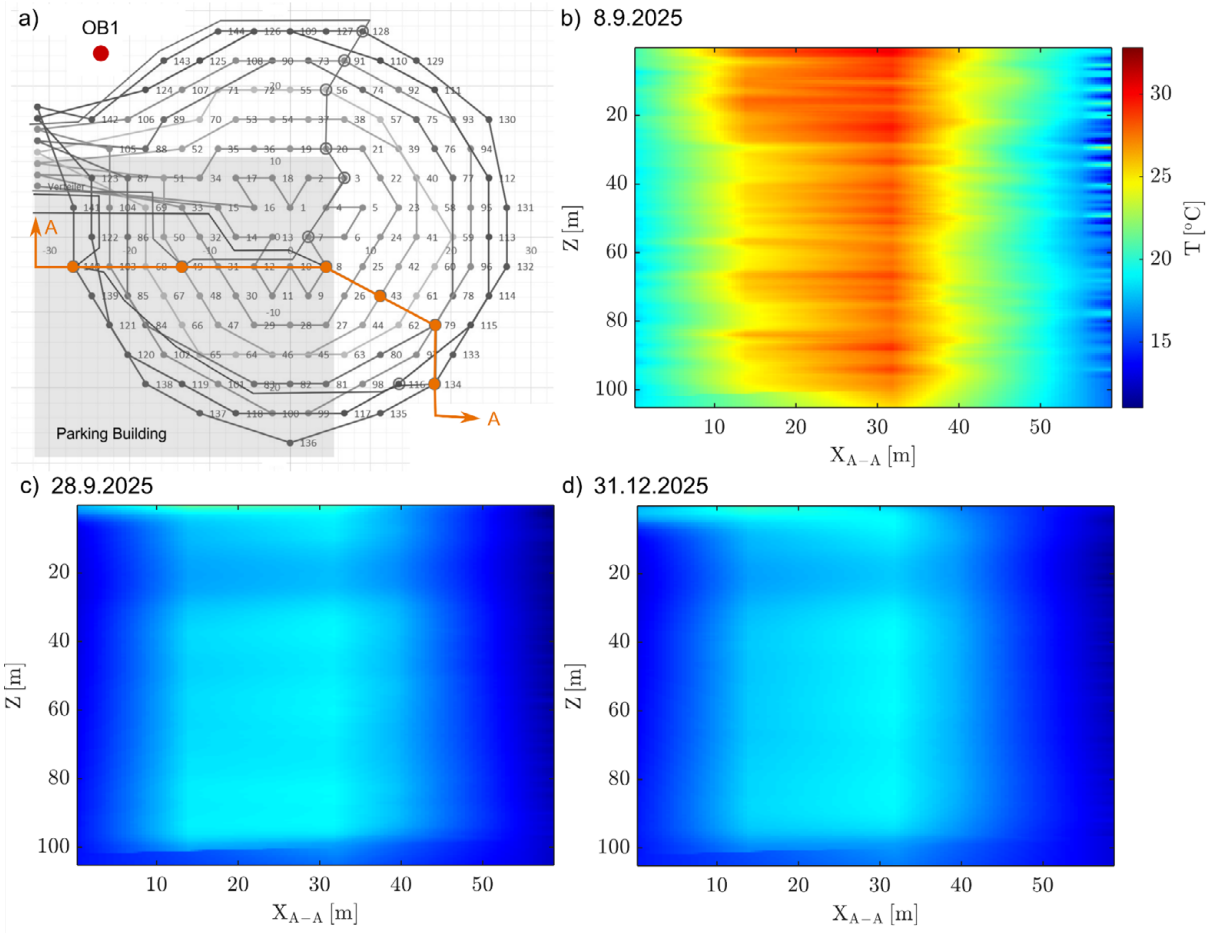

Figure 6. Temporal evolution over depth of the temperature measurements within the HT-BTES facility along a cross section running in west-east direction across the facility. a) Plan view of the cross section A-A. The ground heat exchangers equipped with temperature measurements used to generate the cross section are shown with orange markers. b), c), and d) show the temperature measurements over depth along the cross section A-A for three different dates, 8.9.2025, 28.9.2025, and 31.12.2025, respectively. Panel b) reflects the condition measured at the end of the peak injection period. Panel c) and d) correspond to periods without heat injection. The temperature scale in panel b) is common to all panels.

A numerical simulation of flow and heat transport contracted by Empa during the last quartal of 2025 as part of the permitting requirements for the operation of the HT-BTES facility provided further information for a more accurate estimation of the main groundwater flow direction close to our OBs. This simulation included as input data the time series of *h* shown in Figure 7a, among other sources. Figure 8 summarizes the results of different methods used so far in the project to estimate the groundwater flow direction, where the main outputs of the contracted simulation are shown with the dark blue streamlines (Simultec AG, 2025). Details on the triangulation method and on the Bayesian kriging performed to generate the color and

isoline maps can be found in the 2nd interim report. The results show that the groundwater flow is funneled in the proximity of the HT-BTES facility This bends all streamlines originated both at the upstream observation boreholes (OB2 and OB1) and at the facility towards the OBs localized in the downstream area, OB3 and OB4. This reaffirms the proper localization of these two observation boreholes in order to capture the heat plume as it moves downstream from the facility.

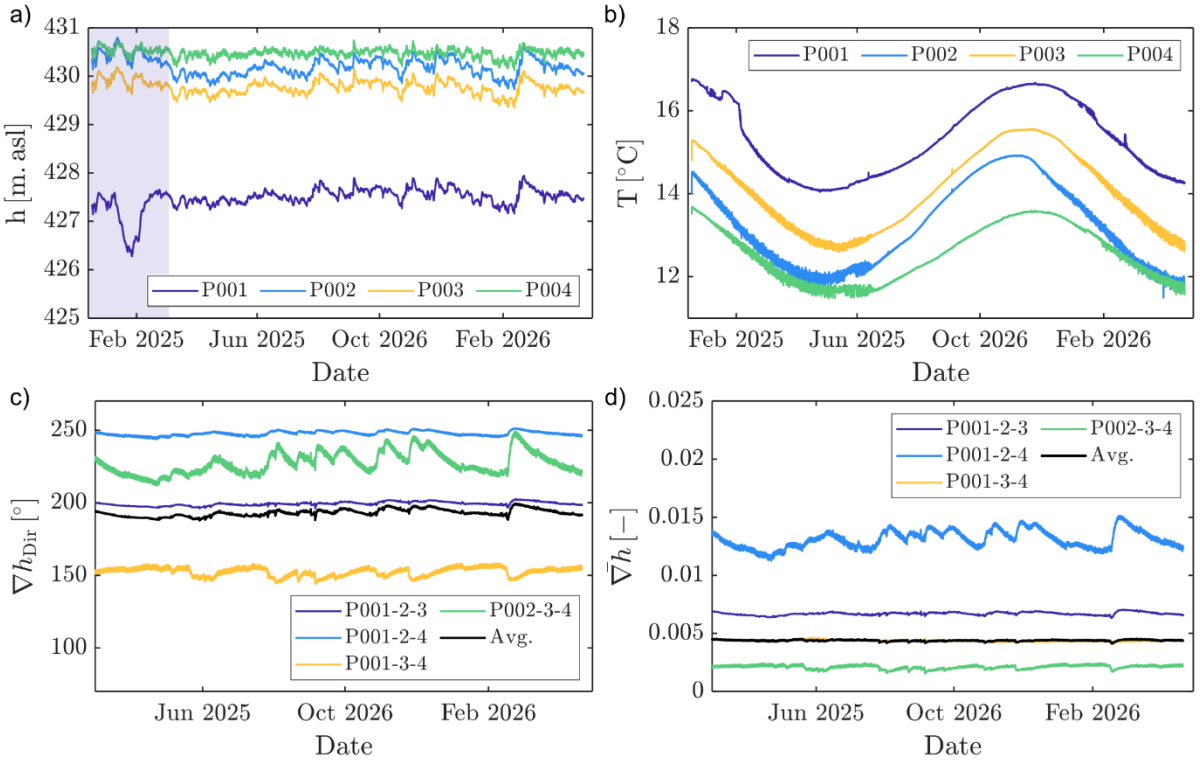

Figure 7. a) Time series of the groundwater levels, *h*, measured from January 2025 up to May 2026 in all four installed piezometers, i.e., P001, P002, P003, and P004. b) and c) Time series of the magnitude, ∇h, and direction, ∇h_{Dir}, of the groundwater gradient, respectively, obtained for all four triangulations performed in the analysis. The time series of the average ∇h and ∇h_{Dir} for the entire project area is shown with the black line. Note that the triangulation P001-2-4 was excluded from the average because of the suboptimal base/height ratio of the resulting triangle. d) Time series of the groundwater temperatures measured at all four monitoring piezometers.

6. Permanent monitoring

6.1 Groundwater physical properties

Figure 9 shows the time series of temperature and electrical conductivity (EC), two of the variables measured continuously in our monitoring concept, from the start of the monitoring activities until the end of June 2026. The time series of temperature at EE1t and EE2t display a clear seasonal variation, with maximum temperature differences between early spring and early autumn of approximately 6 °C. Contrastingly, this seasonal change is not observed at EE3t. We hypothesize that this might be related to the different land cover surrounding this station, which differs from the green area surrounding the other two stations, potentially altering the thermal signal of water infiltrating in proximity to the OB. We also presume that installations placed at the lower levels of the parking house, right in front of which OB3 is located, might have also influenced the temperatures measured at this location.

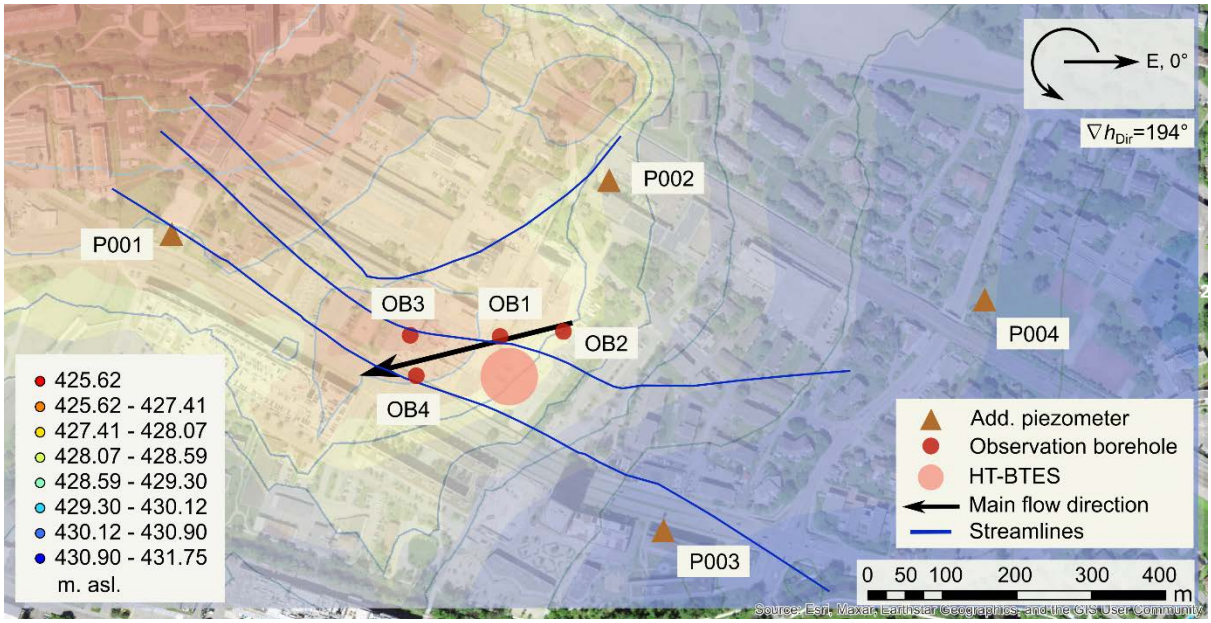

Figure 8. Summary of the regional groundwater flow estimation after integrating results from different methods applied since the beginning of the project. The color map and isolines were obtained from Bayesian kriging performed on a set of single time groundwater level measurements available from infrastructure and housing projects in the area. The black vector represents the resulting groundwater flow direction obtained from triangulation using the data from the piezometers P001, P002, P003 and P004. The corresponding groundwater flow direction as well as the reference system used to interpret it are shown in the upper right corner. Finally, the streamlines show in dark blue were recently generated from a numerical model contracted by Empa for the operation permitting of the facility (Simultec AG, 2025). The location of the observation boreholes, of the monitoring piezometers, and of the HT-BTES facility is also displayed.

Temperature measurements at the upper freshwater molasse show no seasonal variation, which is expected considering the measurement depth of 70 m. However, a steady slow increase has been registered at EE1b since January 2026, amounting to 0.4 °C by the end of June 2026. We believe that this temperature change is a consequence of the first heating cycle in the operation of the HT-BTES. This is supported both by the proximity of EE1b to the facility and by the very similar temperature change registered by the fiber optic within the molasse at the outermost ring of the HT-BTES facility, as shown in Figure 5b.

A more detailed inspection of Figure 9a reveals interesting temperature dynamics since March 2026, which are better displayed in Figure 9d. On one side, temperature increases have only been registered for locations right next to the facility (EE1t) and downstream of it (EE4t), hinting that they might be related to the heat injection. Moreover, EE4t displays a two times larger temperature change than EE1t by the end of the observation period. This might indicate the arrival of the heat plume at the downstream location, where the overall increase of 1.3 °C reflects the dissipation of the temperature change induced at the facility along the flow path towards OB4. We will continue monitoring closely this temperature increase and will evaluate this hypothesis over the coming months through the estimation of local flow velocities as well as heat transport between our monitoring stations.

Figure 9c presents the temporal evolution of EC at all six monitoring locations. Significant changes displayed during March 2026 correspond to the injection of NaBr and NaCl solutions during the tracer tests performed around that time. The latest measurements reflect that the changes in salinity induced by these tests have already been reverted at all stations. No other significant variations in the EC-readings have been registered over the observation period.

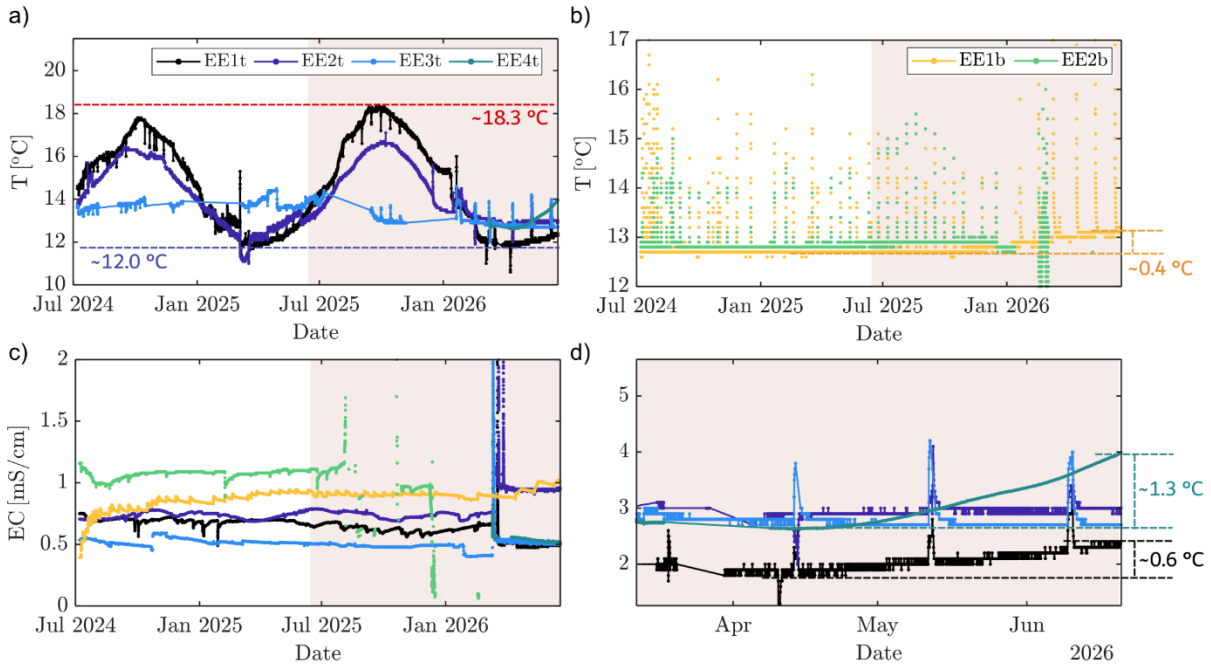

Figure 9. Time series of the groundwater temperature measured at all sampling locations a) within the top aquifer, i.e., EE1t, EE2t, EE3t, and EE4t, and b) within the upper freshwater molasse, i.e., EE1b and EE2b. Panel a) also shows the maximum and minimum temperatures measured over the record period, while panel b) shows the total temperature difference registered so far at EE1b. c) Time series of electrical conductivity, EC, measured for all six sampling locations. Sudden jumps registered during March 2026 were caused by the injection of salt tracers during the tracer tests. d) Evolution of the temperature measurements at all locations within the top aquifer since March 2026. The contrasting temperature differences registered over this time period for EE1t and EE4t are displayed. Single peaks for the time series of EE1t, EE2t,and EE3t are related to the pump operation during sampling days.

6.2 Concentration of dissolved gases

The concentration of dissolved gases was monitored in a continuous manner from July 2024 until December 2025. To reduce the amount of maintenance and increase the reliability of the mass spectrometers installed on site, we switched the measurement frequency to align with the sampling days. Figure 10 shows the time series of four of the measured gas species for the entirety of the sampling period for the stations located at OB1, OB2, and OB3. Note that OB4 is not equipped with a portable mass spectrometer. Gas concentrations at every time point are expressed as partial pressures and have been normalized by the total measured gas pressure. Data points shown with markers belong to the period after the measurement frequency was adjusted.

Overall, the time series show a rather constant behavior for all five sampling locations. No clear seasonal differences are observed either in the top aquifer or in the upper freshwater molasse. Some of the measured species, such as dissolved O_2, show a similar behavior to the results obtained in other sampling activities. This is characterized by the absence of oxygen in the deeper molasse, i.e., EE1b and EE2b, and in the downstream location, EE3t (see Section 7.1).

Changes have so far occurred for the methane concentrations measured in the molasse at the location right next to the facility (EE1b). They have been characterized by a steady increase since the start of the injection, especially pronounced during the winter months, which contrasts with the constant values measured at the upstream location, EE2b. The steeper

change registered since the beginning of 2026 also aligns well with the time window in which temperature changes at EE1b have been registered by our sensors (see Figure 9b). This might indicate that the change in CH_4-concentration is directly linked to the temperature increase induced by the HT-BTES operation in the molasse. We presume that the increase in CH_4-concentrations might be explained by enhanced bacterial activity at this location. First sequencing results obtained for two timepoints at the end of 2024 have revealed an abundance of anaerobic bacterial species in the molasse groundwater, including sulfate reducers (*Desulfuromonadaceae)*. This has been promoted by the anoxic conditions describing the groundwater in this geology. This type of bacteria might play an important role in promoting methanogenesis by breaking down complex organic matter into simpler compounds, which then become available for methanogenic species (Greene, 2014). The registered increase in temperature might be promoting this mechanism (Bonte et al., 2013). This aspect will be further investigated once a longer series of sequencing results becomes available, providing a complete description of the bacterial species encountered in our samples. Further information on the already available sequencing results can be found in the Deliverable 3 and in the 2nd interim report.

It is important to note that the mass spectrometers were out of operation due to malfunctioning and maintenance for significant periods of time during autumn 2024 for the stations located in the molasse, and during the second half of 2025 for all five sampling locations. We expect the operation of the devices to be improved with the change of measurement frequency implemented early this year to avoid further data gaps. Appendix 3 presents the normalized times series of dissolved gas concentrations for all seven measured species until the end of June 2026.

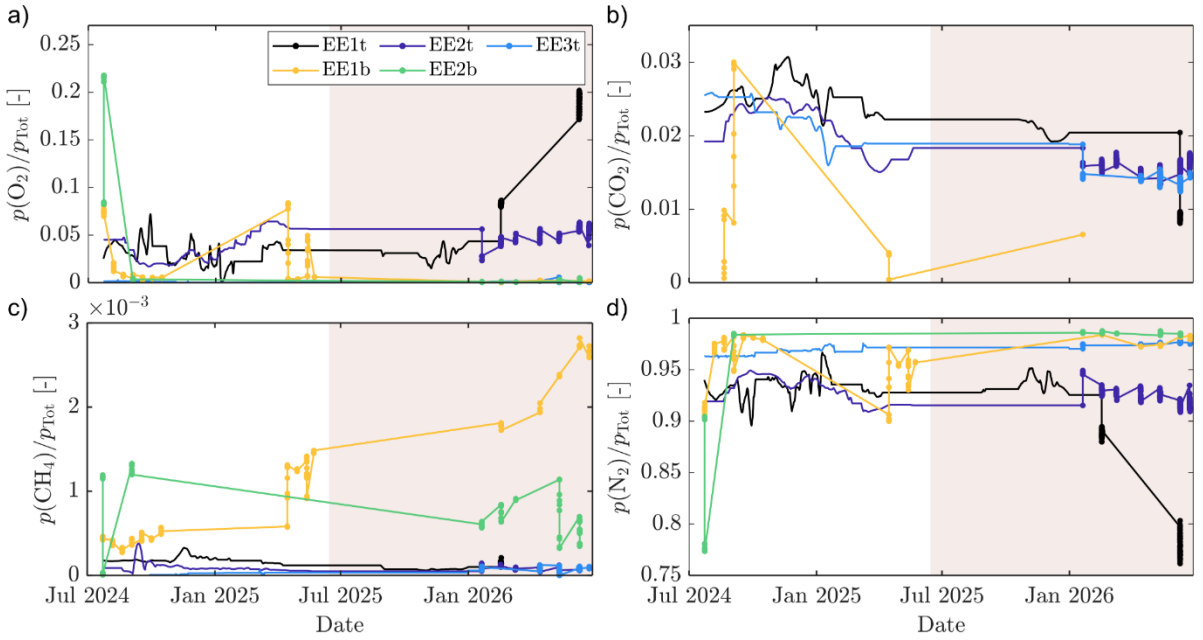

Figure 10. Time series of the concentration of dissolved a) oxygen, O_2, b) carbon dioxide, CO_2, c) methane, CH_4, and d) nitrogen, N_2, for all five sampling locations found in OB1, OB2,and OB3. Note that no mass spectrometer has been installed at OB4. Concentrations are expressed as partial pressures, p(), and they have been normalized by the total gas pressure measured at every time point, p_{Tot}. Data points belonging to time periods in which the devices have not been measuring continuously, that is, since January 2026 for all locations in the top aquifer and since the start of the records for the upper freshwater molasse, are shown with markers. The legend on panel a) is common to all panels. The red hatched area indicates the period since the start of the heat injection.

7. Periodic monitoring

7.1 Groundwater chemistry

7.1.1 Top aquifer of low-terrace gravels and glacial-lake deposits

The second year of monitoring revealed no significant effects on the geochemistry of the top aquifer of unconsolidated glacial-lake deposits and low-terrace gravels. The concentration of all measured element and metal concentrations did not experience drastic changes that could be considered problematic when compared to limits commonly applied for drinking water purposes.

Figure 11 presents a summary of the main variables measured on site during the sampling campaigns. No large variations in pH, electrical conductivity and redox potential have been registered so far, reflecting the stable conditions observed in the concentration time series of all analyzed elements. Low oxygen levels were still registered downstream at EE3t, which contrasts with the higher magnitudes measured since February 2026 at the new downstream borehole EE4t. Figure 12 summarizes some of the measured elements and compounds that have so far described the particular water chemistry encountered at EE3t, namely the concentrations of nitrate, $c(NO_3^-)$, ammonium, $c(NH_4^+)$, and of dissolved iron, c(Fe), and manganese, c(Mn). As observed, these differences in water chemistry across the study site have persisted despite the heat injection. However, EE4t shows in all cases concentrations that resemble the water chemistry found in the upstream locations EE1t and EE2t, differing largely from EE3t. This reassures the conclusion that the water chemistry reported so far for EE3t cannot be generalized for the downstream area, as also concluded from comparison with the results obtained for the piezometers P005 and P006 (see 2nd interim report for details on this comparison). The groundwater chemistry similarity between EE2t, EE1t, and EE4t further supports the conclusion that OB4 will provide valuable information to conclude on the signal that potential geochemical changes taking place at the facility and registered close to it might have in the downstream area.

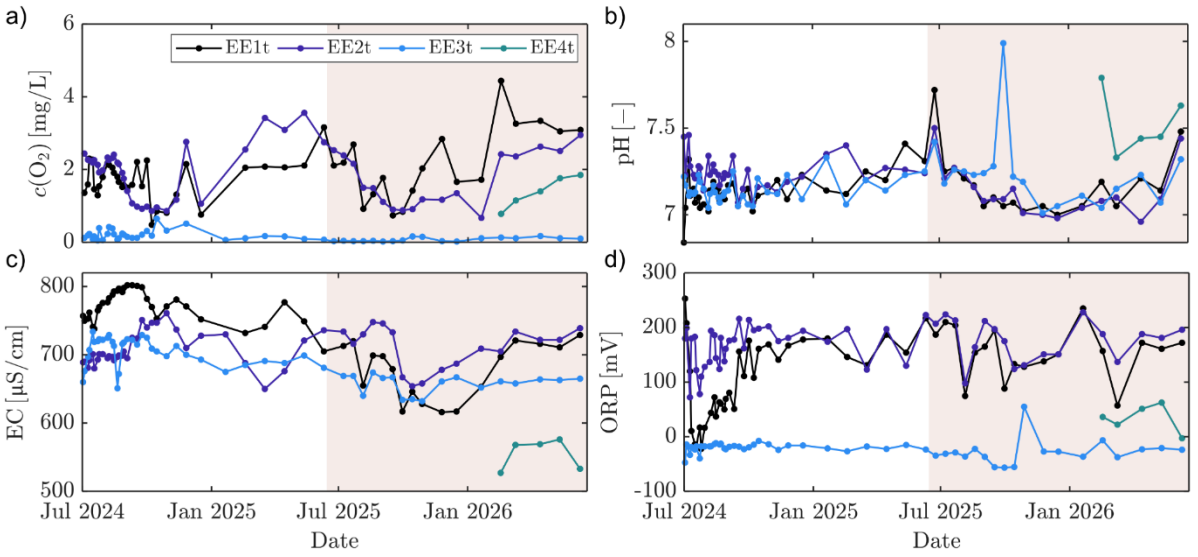

Figure 11. Time series of a) dissolved oxygen concentration, $c(O_2)$, b) pH, c) electrical conductivity, EC, and d) redox potential, ORP, for all sampling locations in the top aquifer of unconsolidated glacial-lake deposits and low-terrace gravels, i.e., EE1t, EE2t, EE3t, and EE4t. The legend on panel a) is common to all panels. The red-hatched indicates the period since the start of the heat injection.

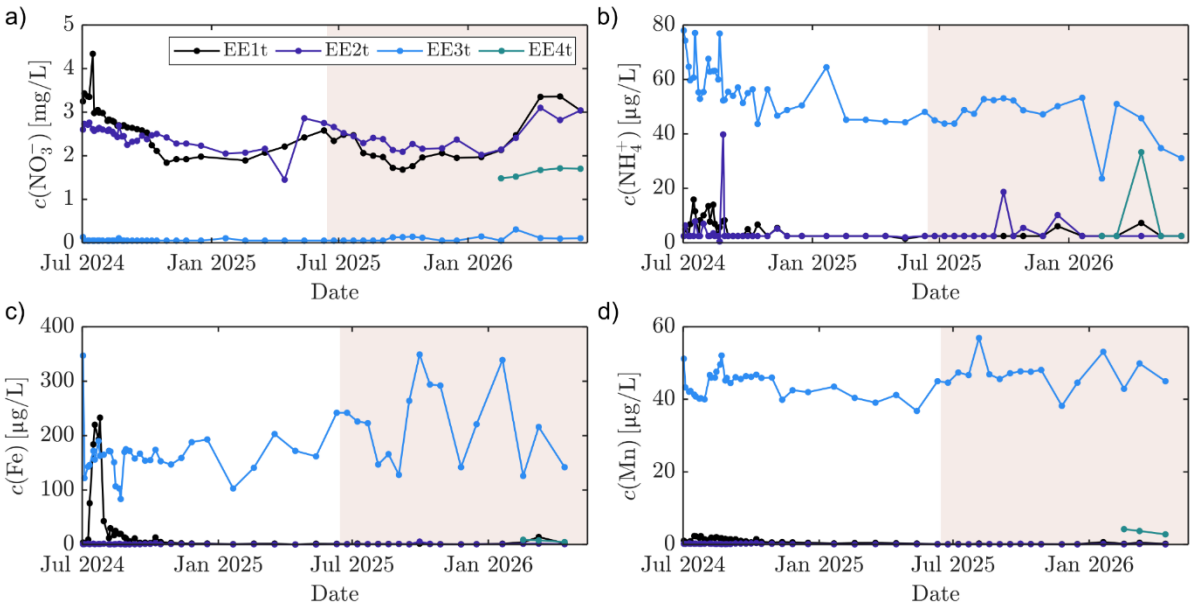

Figure 12. Time series of the concentration of a) nitrate, NO_3^-, b) ammonium, NH_4^+, c) dissolved iron, Fe, and d) dissolved manganese, Mn, measured for all sampling locations in the top aquifer of unconsolidated glacial-lake deposits and low-terrace gravels, i.e., EE1t, EE2t, EE3t, and EE4t. The legend on panel a) is common to all panels. The red-hatched area indicates the period since the start of the heat injection.

Figure 13 shows the time series of concentration of Ca, Ba, V, and Cu. They are examples of two patterns identified in some of the measured compounds. On one hand, the time series of c(Ca) and c(Ba) describe a light seasonality characterized by lower concentrations in the winter months, which has been preserved despite the heat injection. This seasonality has also been observed for the time series of Sr-concentration. On the other hand, Figure 13c and Figure 13d describe cases in which the concentrations close to the facility EE1t have always been larger than those registered upstream in EE2t. This might point out permanent effects on the groundwater chemistry induced by the construction of the HT-BTES facility itself.

During the third year of monitoring activities, we will continue assessing variations in the groundwater chemistry in the top aquifer related to both the expected high-temperature operation of the facility and the arrival of the heat plume to the downstream boreholes. The latter has been hinted already by the temperature measurements registered in EE4t over the last three months of records (see Figure 9d). Appendix 4 presents the full concentration time series of all compounds measured as part of the groundwater chemistry monitoring for the top aquifer. Depending on the type of analysis used for their quantification, they include data until either the end of April 2026 or the end of May 2026.

7.1.2 Upper freshwater molasse

In contrast to the groundwater sampled from the top aquifer of unconsolidated glacial lake deposits and low-terrace gravels, some of the monitored compounds and element concentrations in the upper freshwater molasse have experienced considerable changes since the beginning of the HT-BTES operation.

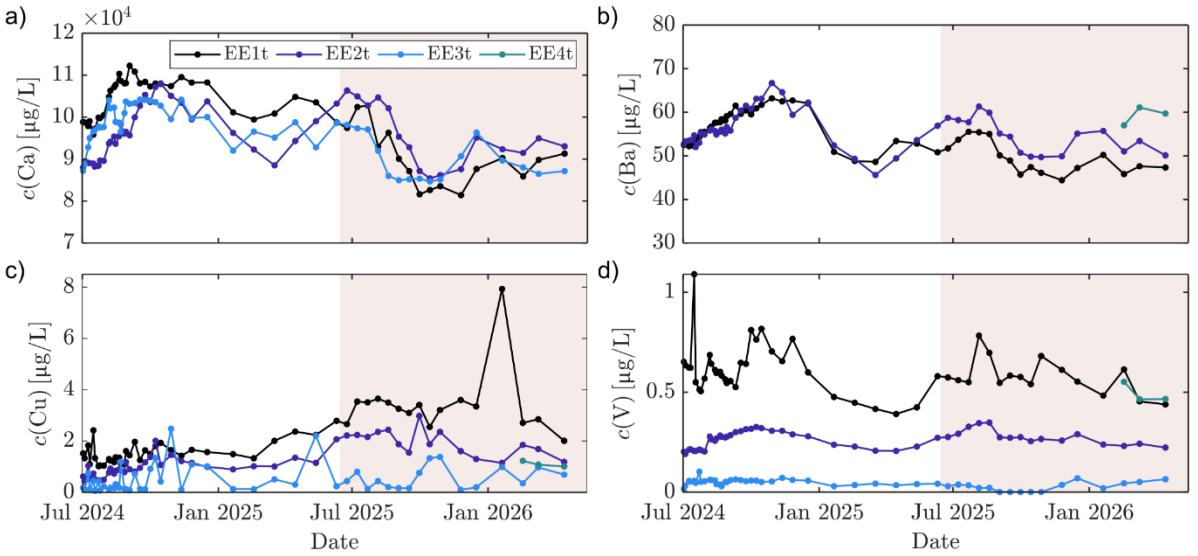

Figure 13. Time series of the concentration of dissolved a) calcium, Ca, b) barium, Ba, c) cupper, Cu, and d) vanadium, V, for all sampling locations in the top aquifer of unconsolidated glacial-lake deposits and low-terrace gravels, i.e., EE1t, EE2t, EE3t, and EE4t. The legend on panel a) is common to all panels. The red-hatched area indicates the period since the start of the heat injection.

Figure 14 shows the full time series of some of the key variables measured on site during sampling. Overall, they reflect few to no changes since the first heat injection. Single exceptions include the sudden increase of EC measured for EE2b in May 2026, which was caused by the tracer test performed at this location during the second week of April. Due to the lower groundwater flux in the molasse, which conditions the maximum allowed pumping duration, a full extraction of the injected salt tracer (NaCl) from both the borehole water and the surrounding groundwater was not possible during the extraction phase of the test. Figure 14b also shows a slow but steady decrease in pH values in EE1b, which sets in shortly after the start of the heat injection.

Further results also indicate a clear increase in the concentration of some elements and trace metals since the start of the heat injection. Figure 15 presents the time series of the concentrations of Ba, Ca, Fe, and Mn. They all display a fast increase in concentration shortly after the start of the injection, followed by a slow decrease during summer and autumn. By January 2026, concentrations reach similar values to those measured prior to the injection in all cases. Considering that the overall temperature change in this geology at the outermost ring of the HT-BTES facility was approximately 0.6 °C, with maximum variations of approximately 6 °C during the period of peak injection, our results show a very sensitive groundwater chemistry in the molasse, with a fast response to temperature variations.

The increase in c(Ca) depicted in Figure 15b suggests an enhanced calcite dissolution process, which seems unexpected considering its retrograde solubility upon changes in temperature. We thus believe that this increase is associated with other geochemical and biochemical reactions. The increase in c(Fe) and c(Mn) shown in Figure 15c and Figure 15d, respectively, can be explained by an enhancement of the microbial activity at this geology, as previously hinted in Section 6.2. In particular, the abundant presence of *Comamonadaceae* and *Desulfuromonadaceae* in the molasse rock, which we identified with sequencing data of two time points at the end of 2024, can be driving these changes (see interim report 2 for a detailed analysis of this data set). *Comamonadaceae,* as a very diverse phenotype, includes anaerobic denitrifies and Fe-reducing bacteria (Willems, 2014), whereas *Desulfuromonadaceae* directly mediates dissimilatory metal reduction, for which both Fe and

Mn are commonly chosen electron acceptors (Greene, 2014). We will be able to provide a more detailed analysis of the interaction between microbiology and groundwater chemistry driving temperature-induced changes in our observations once that a full time series of DNA-sequencing becomes available. This is expected to occur in fall 2026.

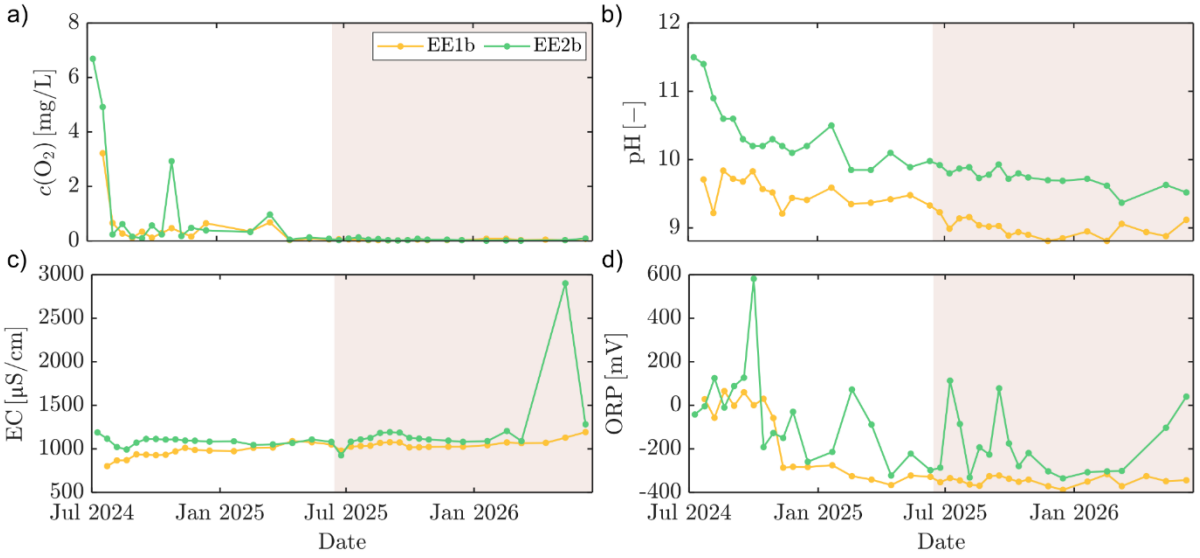

Figure 14. Time series of a) dissolved oxygen concentration, c(O_2), b) pH, c) electrical conductivity, EC, and d) redox potential, ORP, for all sampling locations in the upper freshwater molasse, i.e., EE1b and EE2b. The legend on panel a) is common to all panels. The red-hatched area indicates the period since the start of the heat injection.

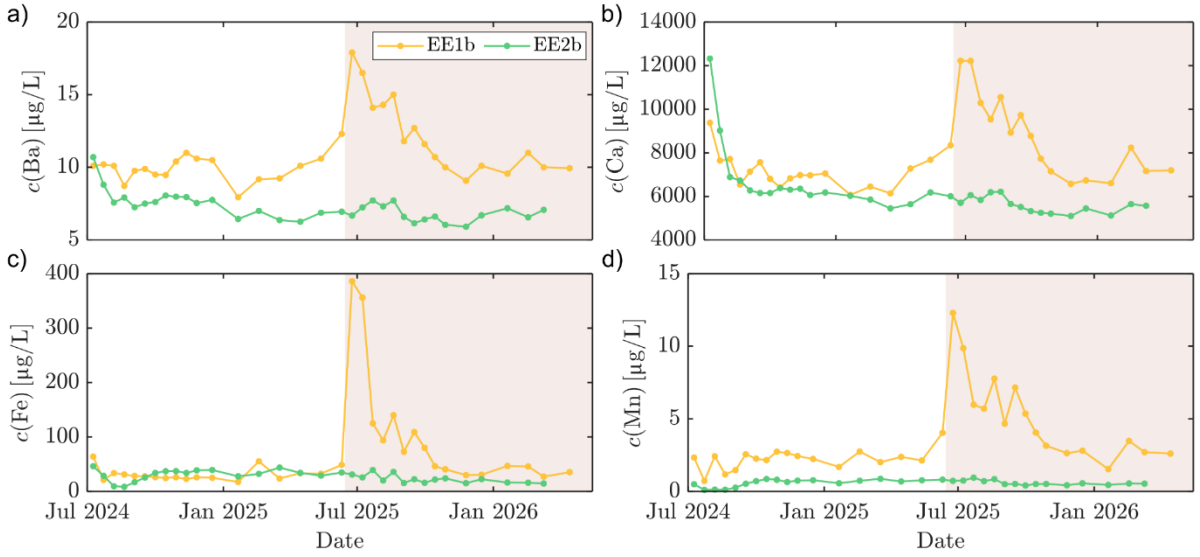

Figure 15. Time series of the concentration of dissolved a) barium, Ba, b) calcium, Ca, c) iron, Fe, and d) manganese, Mn, for all sampling locations in the upper freshwater molasse, i.e., EE1b and EE2b. The legend on panel a) is common to all panels. The red-hatched area indicates the period since the start of the heat injection.

7.2 Microbiology

During the second year of the ARTS project, we continued the regular groundwater sampling campaign for microbiological characterization across all five, and later six, monitoring locations. We perform two types of microbiological analyses. First, microbial cell concentrations are determined by flow cytometry on the day of sampling. Second, microbial community composition is characterized by sequencing of the 16S rRNA gene. For the latter, samples are stored at –80°C immediately after collection and processed in larger batches. Progress on both analyses is summarized below.

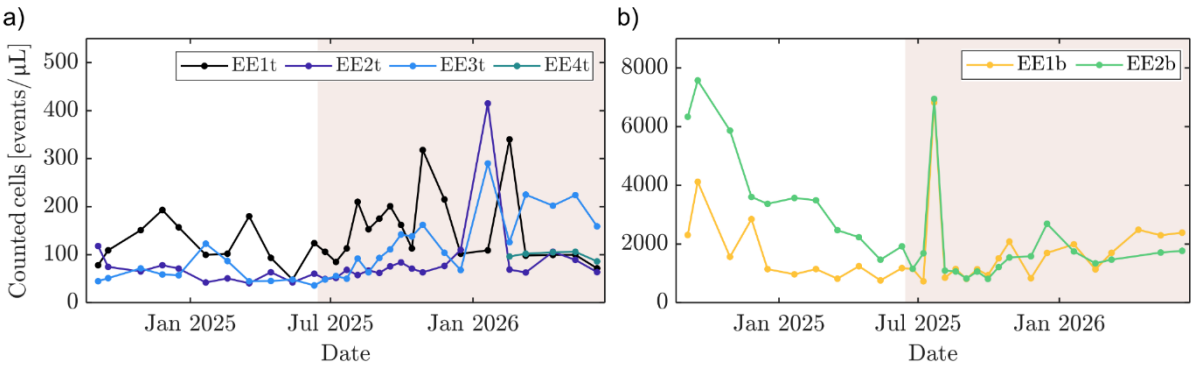

Figure 16. Microbial cell concentrations determined by flow cytometry. To distinguish microbial cells from abiotic debris, a fluorescent DNA stain was applied, and particles were gated based on their green fluorescence intensity and a related signal in the red fluorescence channel typical for microbial cells. Only particles most likely to represent microbial cells were included in the counts shown here. The red-hatched area indicates the period since the start of the heat injection.

To quantify microbial cell concentrations, groundwater samples are stained with the DNA-specific fluorescent dye SYBR Green and analyzed by flow cytometry. This staining facilitates the distinction between microbial cells and abiotic particles, although some autofluorescent non-biological particles may still be included in the counts. As shown in Figure 16, cell concentrations in the shallow boreholes continue to exhibit considerable temporal variability, ranging from approximately 50 to 400 cells/µL. In contrast, concentrations in the deeper boreholes appear to have stabilized, remaining within a narrower range of approximately 1000 to 2000 cells/µL.

To characterize microbial community composition in the groundwater, DNA extraction has been initiated for samples collected between July 2024 and January 2026, including at least one sample every two months. DNA concentrations are quantified using a Qubit fluorometer, and total DNA yields obtained from the collected 0.2 to 10 liters of groundwater are calculated. Among the upper boreholes, DNA yields per liter were highest in EE1t, intermediate in EE2t, and lowest in EE3t (Figure 17a), mirroring the patterns observed for cell concentrations (Figure 16). The DNA yields per liter of groundwater were initially much higher than for the bottom boreholes but decreased significantly over time, likely indicating that the ecosystem in these boreholes took longer to equilibrate after being perturbed during the installation. Comparison of DNA yields and cell concentrations per groundwater sample revealed significant correlations for both the upper boreholes (R^2 = 0.39) (Figure 17b) and the lower boreholes (R^2=0.90, provisionally removed three timepoints as outliers) (Figure 17d).

DNA extraction of the remaining samples is expected to be completed by the end of July 2026. Subsequently, all samples will be submitted for 16S rRNA gene amplicon sequencing using the widely adopted primer pair 515F/806R to assess microbial community composition and

dynamics across this first monitoring period. We anticipate that the sequencing results will be available in fall 2026.

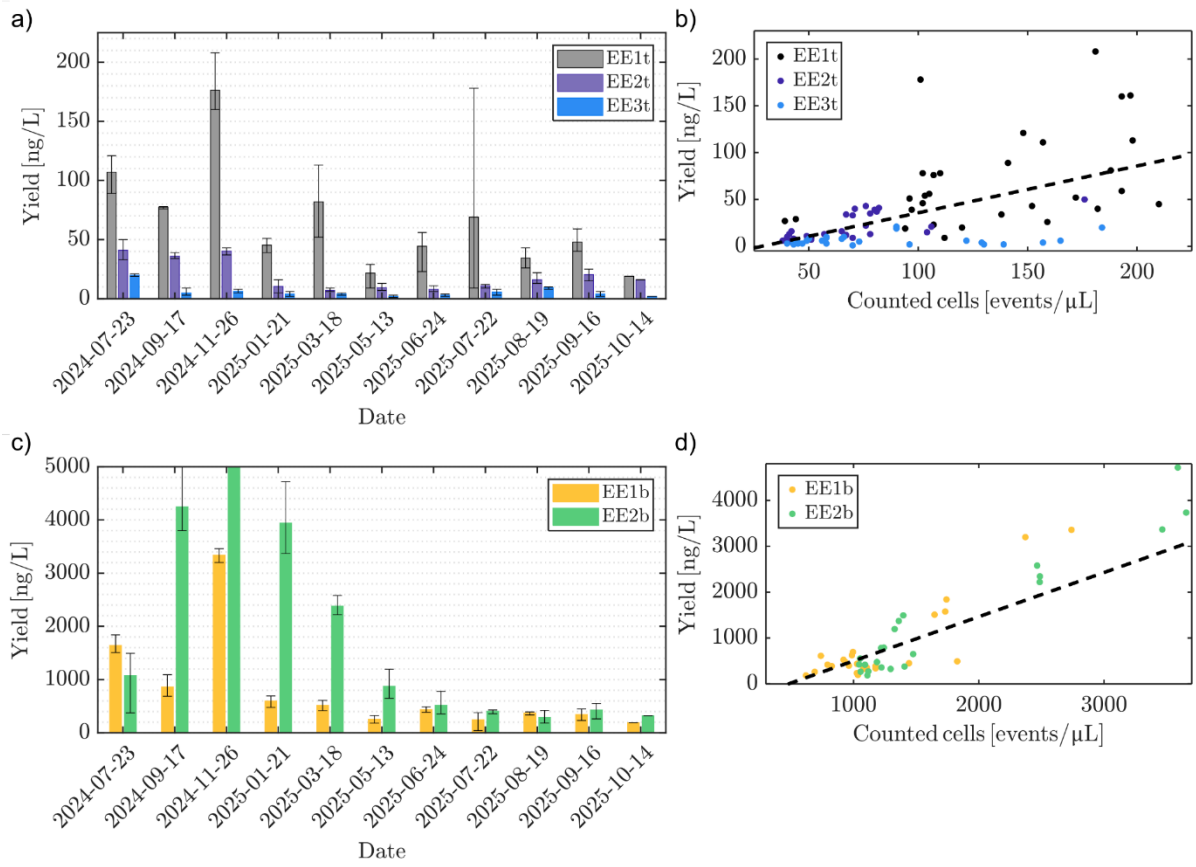

Figure 17. DNA extraction results from groundwater samples collected at 11 selected time points over the past two years. a) Total DNA yield per liter of groundwater of selected timepoints for the top aquifer of low-terrace gravels and glacial-lake deposits. Note that there are three replicates per sampling location and timepoint, with error bars indicating the standard deviation. b) Correlation between the DNA yield results shown in panel a) to microbial cell concentrations determined by flow cytometry for the same timepoints. Panels c) and d) show the same type of analysis a) and b) for the samples collected at the upper freshwater molasse. The vertical axis in c) is capped at 5000 ng/L for improved visualization. Note that for panel d), only the 2025 timepoints, excluding 2025-07-22, were included in the correlation analysis because the others represented strong outliers relative to the remaining observations; the cause of these deviations has not yet been resolved and is being investigated further.

7.3 Environmental DNA

To understand the effects of heat injection in the upper and lower aquifers on groundwater biodiversity and ecology (fauna and fungi), environmental DNA (eDNA) samples are taken since July 2024 on a bi-weekly basis. This constitutes of filtering water onsite through Sterivex™ filters with a filter pore size of 0.22 µm (compare Figure 19a in Deliverable 3). Up to this point, there are 33 timepoints sampled, each covering the five sampling locations shown in Figure 1a. From February 2026 onwards, sampling of the newly drilled observation borehole 4 (EE4t) was conducted. Filtrations on-site are done in three replicates, each consisting of groundwater volumes between 500 mL and 5 L, depending on sediment load.

Currently, eDNA is extracted from filters for every other timepoint. This allows tracking temporal dynamics while providing an insight where to increase analysis intervals. The first next-generation sequencing (NGS) library was prepared in spring 2026. Preparation of an

eDNA library includes DNA amplification using polymerase chain reaction (PCR), tagging and pooling samples for subsequent sequencing on the NGS platform. In the first round, two libraries using two different markers were prepared. The different genetic markers aim to recover different organismal groups, covering different branches of the tree of life. The marker Crust16S amplifies and recovers eDNA from crustacea, while the ITS marker amplifies and recovers eDNA from fungi. Whereas the sequencing of the ITS marker worked well, the results for Crust16S yielded very low DNA, insufficient for further sequencing. While adjustments to lab protocols are ongoing, eventually a switch to the 18S marker is considered, dropping the aimed amplification of Crust16S. The marker 18S has been shown to work very well and recover a wide diversity of metazoan diversity.

The resulting sequence lengths for the ITS sequencing are within the target range (target = 314 bp, range 270–405 bp). The bioinformatic pipeline demultiplexes the raw reads based on tags, removes primers, pairs reads, removes mismatched pairs, and corrects sequencing errors using UNOISE3. Sequences were clustered into ASVs (amplicon sequence variants) and consecutively into OTUs (operational taxonomic units).

Based on these first categorizations, analyses revealed a low diversity of fungi in the upper freshwater molasse (range: 0–21 OTUs after initial sampling) with high temporal consistency, while showing higher diversity and temporal fluctuations in the top aquifer (range: 0–60 OTUs after initial sampling and without one outlier date). The general diversity is in the range of zero to a few dozen OTUs or ASVs (Figure 18). The large variability at the start of the record period, particularly for the molasse, has also been observed in the concentration time series of several elements included in the groundwater chemistry analysis. This suggest that some degree of mixing between the groundwater of both geologies and/or some contamination form the drilling works was still visible in the sampled water. Later samples showed a clearer picture with an overall lower diversity. The upstream borehole OB2 shows intermediate richness in fungi, with signals of low diversity even in the freshwater molasse (middle panel). In contrast, OB1 reveals consistently higher fungal richness in the top aquifer, while the freshwater molasse also seems very low in diversity (left panel). The downstream borehole with a very specific groundwater chemistry shows very little OUT richness (right panel).

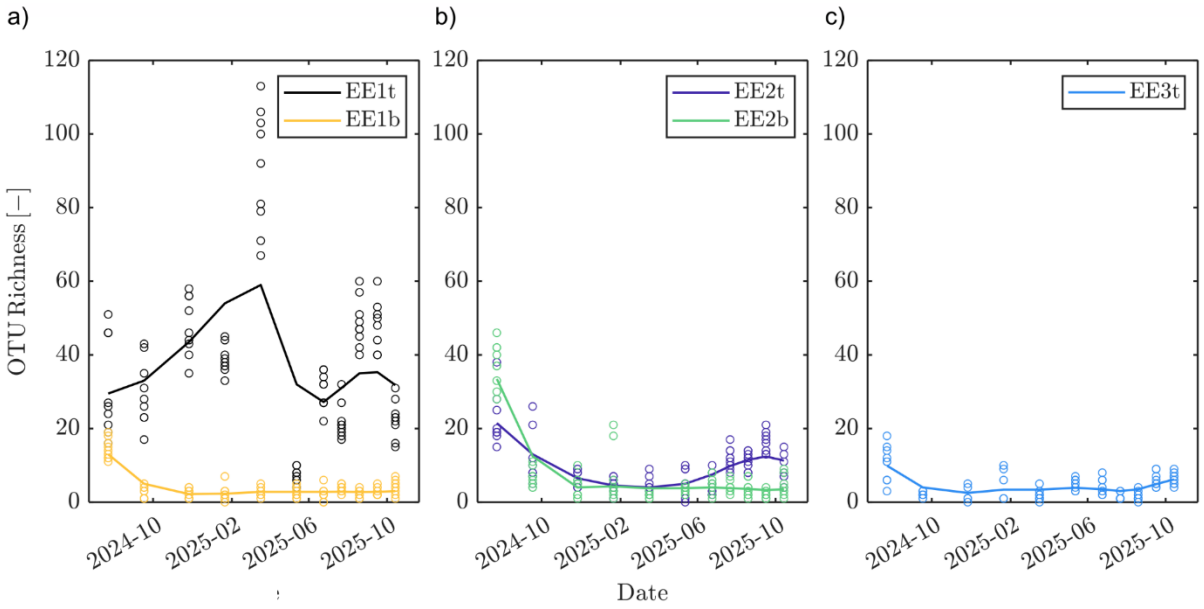

Figure 18. Temporal patterns of biological richness (operational taxonomic units, OTUs) obtained from samples at specific timepoints for the sampling locations in a) OB1, b) OB2, and c) OB3.

The results are very preliminary and should be treated with caution. The taxonomic assignment into biological entities such as families, genera, or species is pending. This step is needed to confirm that the found diversity corresponds to fungi. Also, the data does not yet span into winter 2025/2026. Clear signals of the heat injection on groundwater biodiversity are therefore still pending, while the general suitability of the method is proven.

8. Conclusions

After a first year of monitoring dedicated to the description of the undisturbed aquifer conditions, the second monitoring year offered the opportunity to monitor closely the effects of the first heat injection on the subsurface. This first injection was performed in a mid-temperature range (maximum injection temperatures of 38 °C) in relation to the maximum expected injection temperatures of 65 °C. Compared to the undisturbed condition, this resulted in a maximum temperature increase at the edge of the facility of 6 °C during the peak injection periods, and of 0.6 °C during the winter months. In contrast, temperature changes inside of the facility reached 16 °C and 6 °C during these two periods, respectively

The monitoring results overall reflect a mild effect of the abovementioned temperature changes on the subsurface. In particular, the top aquifer of low-terrace gravels and glacial-lake deposits did not experience significant changes in any of the monitored variables. This might be explained by the constant groundwater flux in this geology, which dampens the thermal signal due to both the mixing of heated and incoming groundwater and the dispersion of the heat plume downstream of the facility. This overall reduces the temperature gradients across the area as well as the residence time of groundwater in regions of high temperature.

Groundwater in the upper freshwater molasse at the location close to the facility (EE1b) revealed some interesting changes during the summer and autumn seasons. The induced temperature changes were enough to induce variations in the concentrations of some trace metals, i.e., Fe and Mn, and of some additional elements, such as Ba and Ca. Additionally, a constant increase in the concentration of dissolved methane has been observed since the beginning of the injection. These changes point to complex biogeochemical interactions, which can be closely related to the bacterial community composition in that geology. This composition is described by anaerobic bacterial species known for inducing dissimilatory metal reduction, with Fe and Mn being common targets (Greene, 2014), and for potentially mediating the activity of methanogens through the degradation of organic matter (Greene, 2014). The measured temperature increase can thus enhance the activity of these communities. However, it is important to note that most of the observed effects were reverted during the winter period, although a temperature change has remained within the molasse since the heat injection finished. The only exception is the concentration of dissolved methane, which has shown a constant increase since the start of the injection. A full set of DNA-sequencing results both for microbiology and ecology will provide essential tools for improving our conclusions on the observed changes.

We will continue monitoring and assessing the aquifer dynamics during the second heat injection. We will pay particular attention to the effects already observed in the past year to conclude on their occurrence in direct relationship with the heating cycle. We will also pay special attention to potential effects on our two downstream observation boreholes. This responds to the apparent arrival of the heat plume at these locations indicated by the temperature measurements registered at EE4t over the past three months. Concluding on the potential effects downstream of the facility will be essential for the goals of the ARTS project with regards to the sustainable implementation of high-temperature underground heat storage.

References

Bonte, M., Röling, W.F.M., Zaura, E.,van der Wielen, P.W.J.J., Stuyfzand, P.J., van Breukelen, B.M. (2013). Impact of shallow geothermal energy production on redox processes and microbial communities. *Environmental Science & Technology,* 47, 14476-14484.

Devlin, J., and Schillig, P. (2017). HydrogeoEstimatorXL: an Excel-based tool for estimating hydraulic gradient magnitude and direction. *Hydrogeology Journal*, 25(3), 867-875.

Greene, A.C. (2014). The Family Desulfuromonadaceae. In: Rosenberg, E., DeLong, E.F., Lory, S., Stackebrandt, E., Thompson, F. (eds) The Prokaryotes. Springer, Berlin, Heidelberg.

Moeck, C., Affolter, A., Radny, D., Dressmann, H., Auckenthaler, A., Huggenberger, P., and Schirmer, M. (2018). Improved water resource management for a highly complex environment using three-dimensional groundwater modelling. *Hydrogeology Journal*, 26(1), 133–146.

Moeck, C., Merk. M., Radny, D., Auckenthaler, A., Schirmer. M., and Gabriel, T. (2022). Eine Echtzeit-Online-Methode zur Beurteilung der künstlichen Grundwasseranreicherung und Grundwasserentnahme. *Grundwasser*, 27(3), 187–196.

Simultec AG (2025). EMPA, Projekt «Nest»: Grundwassermodellierung EWS/Feld, Nachführung Strömungsmodell.

Willems, A. (2014). The Family Comamonadaceae. In: Rosenberg, E., DeLong, E.F., Lory, S., Stackebrandt, E., Thompson, F. (eds) The Prokaryotes. Springer, Berlin, Heidelberg.

Appendix 1: Photographic record of the material core extracted from the observation borehole 4 (OB4)

0 – 3 m

3 – 6 m

6 – 9 m

9 – 12 m

12 – 15 m

15 – 18 m

18 – 21 m

21 – 24 m

24 – 27 m

27 – 30 m

30 – 33 m

33 – 36 m

36 – 39 m

Appendix 2: Lithological column for the observation borehole 4 (OB4)

ARTS - Aquifer Reaction to Thermal Storage

Auftraggeber:
Eawag, Überlandstrasse 133, 8600 Dübendorf
Empa, Überlandstrasse 129, 8600 Dübendorf

Bohrunternehmung:
KIBAG Bohrungen AG, Bächaustrasse 73, 8806 Bäch

Geologische Begleitung:
Aufnahme: Dr. Lawrence Och, AfU TG
10. bis 12. Dezember 2025

SONDIERBOHRUNG NR. 4

Höhenlage: 432.46 m ü.M.
Koordinaten: 2'688'579.1 / 1'250'779.8
Neigung: vertikal
Bohrart: Kernbohrung

Bohrprofil Massstab 1 : 100

Ausführungsdatum: 5. bis 11. Dezember 2025

Bohrmeister: Burhan Ismaili

Koten Höhen [m ü.M.]	Tiefen ab OKT	Profil	Schichtbeschrieb	Geologische Identifikation	Ausbeute
	1.00		Humus, tonig-siltig, durchwurzelt, braun, darunter Kies, sandig, schwach siltig, oben reichlich Steine bis ø 10 cm, beige	künstliche Aufschüttung	100%
429.45	3.00		Sand (vorw. feinkörnig), stark siltig, kiesig, schwach tonig, reichlich Steine bis evtl. Blöcke, polymikt (u.a. mikrit. Kalkstein, Sandstein, roter Tonstein), beige-braun		
	3.60		Sand, (vorw. mittelkörnig), stark kiesig, schwach siltig, grau	Niederterrassen-schotter	
	5.30		Sand (vorw. mittelkörnig, Korngrösse tendenziell nach unten zunehmend), schwach kiesig bis nur vereinzelt Kieskomp., evtl. lagenweise tonig-siltig (mögl. Bohreffekt), bräunlich-grau		
	6.10		Sand (oben v.a. grob-, unten v.a. mittelkörnig), schwach siltig, schwach kiesig, grau		
	6.80		Sand (vorw. fein- bis mittelkörnig), schwach siltig bis siltig, beige		
	7.00		Silt, tonig, fein geschichtet, kompakt, hellbeige		
	7.55		Sand (vorw. fein- bis mittelkörnig), schwach siltig, wenig Steine bis ø 8 cm, kantengerundet, grau-beige		
	8.20		Sand (vorw. feinkörnig), schwach siltig, beige		
	9.00		Sand, stark siltig, schwach kiesig bis kiesig, schwach tonig, wenig Steine, angerundet, polymikt, beige		
	9.30		Sand (vorw. mittelkörnig), schwach siltig, kiesig, wenig Steine bis ø 8 cm, kantengerundet, beige		
	12.75		Sand, stark kiesig, schwach siltig, schwach tonig, mässig Steine bis ø 12 cm, kantengerundet bis gerundet, polymikt, teilw. kantige Tonschiefer, teilw. poliert, beige-grau		
	13.80		Sand, stark kiesig, schwach tonig-siltig, wenig Steine bis ø 8 cm, teilw. poliert und gekritzt, grau-dunkelgrau		
416.85	15.60		Sand (vorw. feinkörnig), stark siltig, stark kiesig, schwach tonig, wenig Steine bis ø 8 cm, kantengerundet bis angerundet, grau		
	18.80		Sand (feinkörnig), siltig bis v.a. stark siltig, schwach tonig, schwach kiesig, Steine bei ca. 17.90 m (ø>12 cm) und 18.80 m (ø<12 cm), kantengerundet, polymikt, grau-beige	eiszeitliche Seeablagerungen	
	22.10		Sand (vorw. feinkörnig), schwach siltig, schwach tonig, vereinzelt Kies, beige und grau		
	22.70		Sand (vorw. mittel- bis grobkörnig), schwach siltig, kiesig, Komp. kantengerundet bis angerundet, grau		
	25.45		Sand (vorw. feinkörnig), schwach siltig, mehrere cm-mächtige siltige Zwischenlagen, gegen unten zunehmend mittelkörnig, beige		
	26.30		Sand (vorw. mittel- bis grobkörnig, mit roten und grünen Körnern), evtl. grob geschichtet, schwach siltig, beige-grau		
	27.00		Sand (feinkörnig), siltig bis stark siltig, schwach tonig, vereinzelt Kies und Steine bis ø 8 cm, teilw. poliert, beige		
	29.70		Sand (feinkörnig), stark siltig, schwach tonig, vereinzelt Kies, lagenweise schwach kiesig, Komp. poliert, teilw. Schichtung erkennbar, ca. 28 bis 29 m: kompakt, ansonsten zerbohrt, beige-grau		
401.40	31.05		Sand (vorw. feinkörnig), schwach siltig, grau-beige		
	37.80		Sand (feinkörnig), siltig bis stark siltig, kiesig (lagenweise schwach kiesig), schwach tonig, wenig bis lagenweise reichlich Steine (32.2 bis 33.0 m), evtl. Blöcke, polymikt, teilw. poliert und gekritzt, vorw. dunkle Komponente, fest, unterhalb 33 m zerbohrt, beige, oben gräulich beige	Moräne	
394.25					
394.45	38.00		Sandstein, hart, angewittert, evtl. mit Grabgängen, rötlich-beige-grau	OSM	

Bemerkungen

4.5"-Piezo:

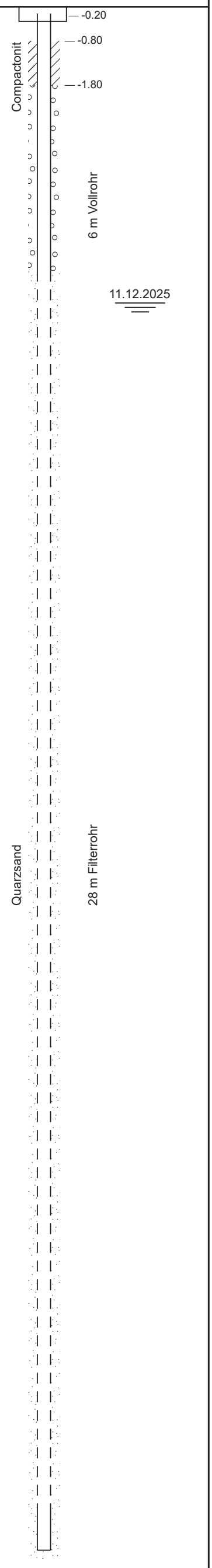

Appendix 3: Summary of the time series of the concentration of dissolved gases

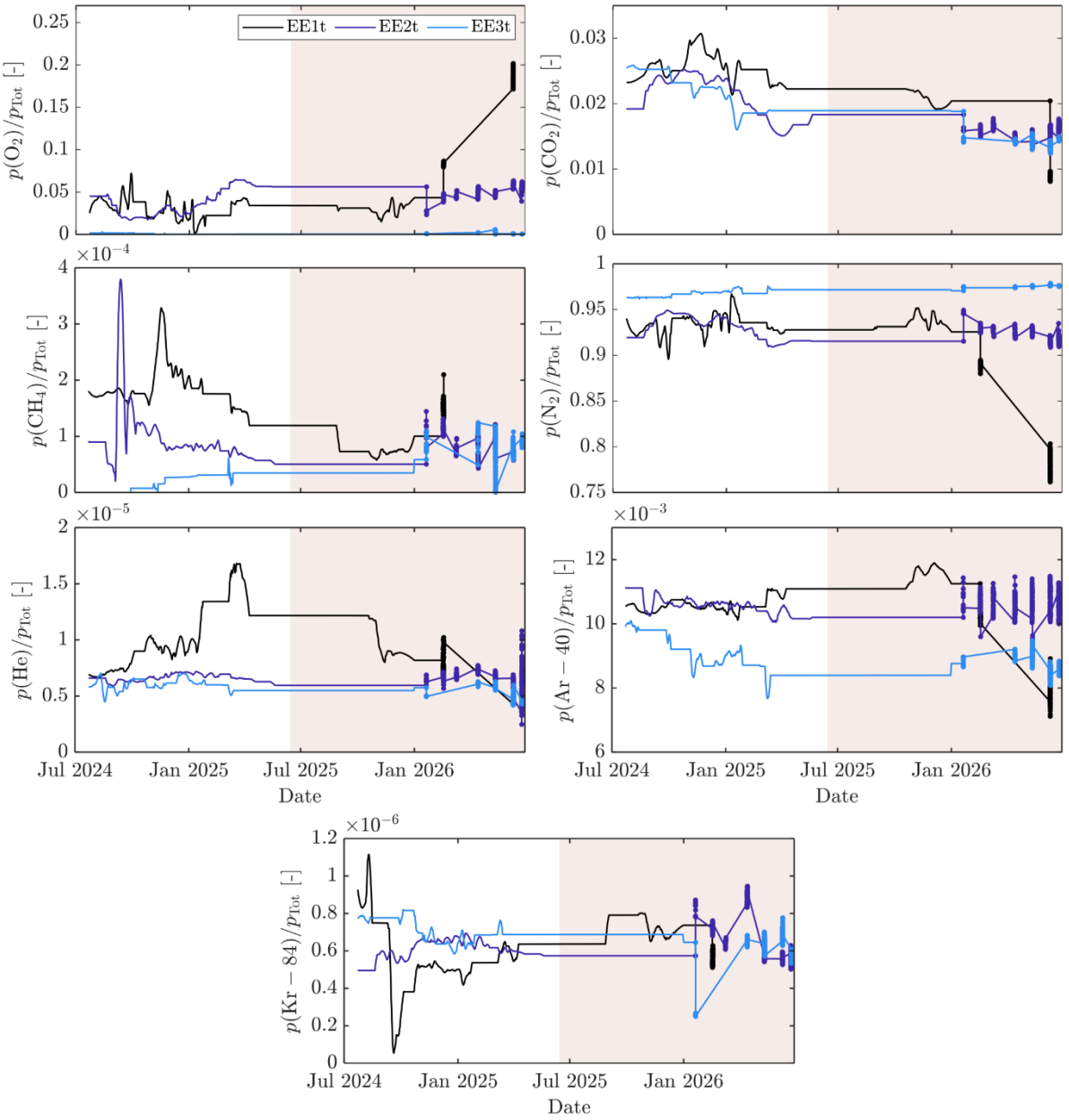

Figure A1. Time series of the concentration of dissolved gases measured in all three sampling locations belonging to the top aquifer of low-terrace gravels and glacial-lake deposits, i.e., EE1t, EE2t, and EE3t. All concentrations, expressed as partial pressures, have been normalized by the total gas pressure, p_{Tot}, measured at each time point. Measured species include dissolved oxygen (O_2), carbon dioxide partial pressure (CO_2), methane (CH_4), dissolved nitrogen (N_2), helium (He), argon-40 (Ar-40), and krypton-84 (Kr-84). The red-hatched area indicates the period since the start of the heat injection.

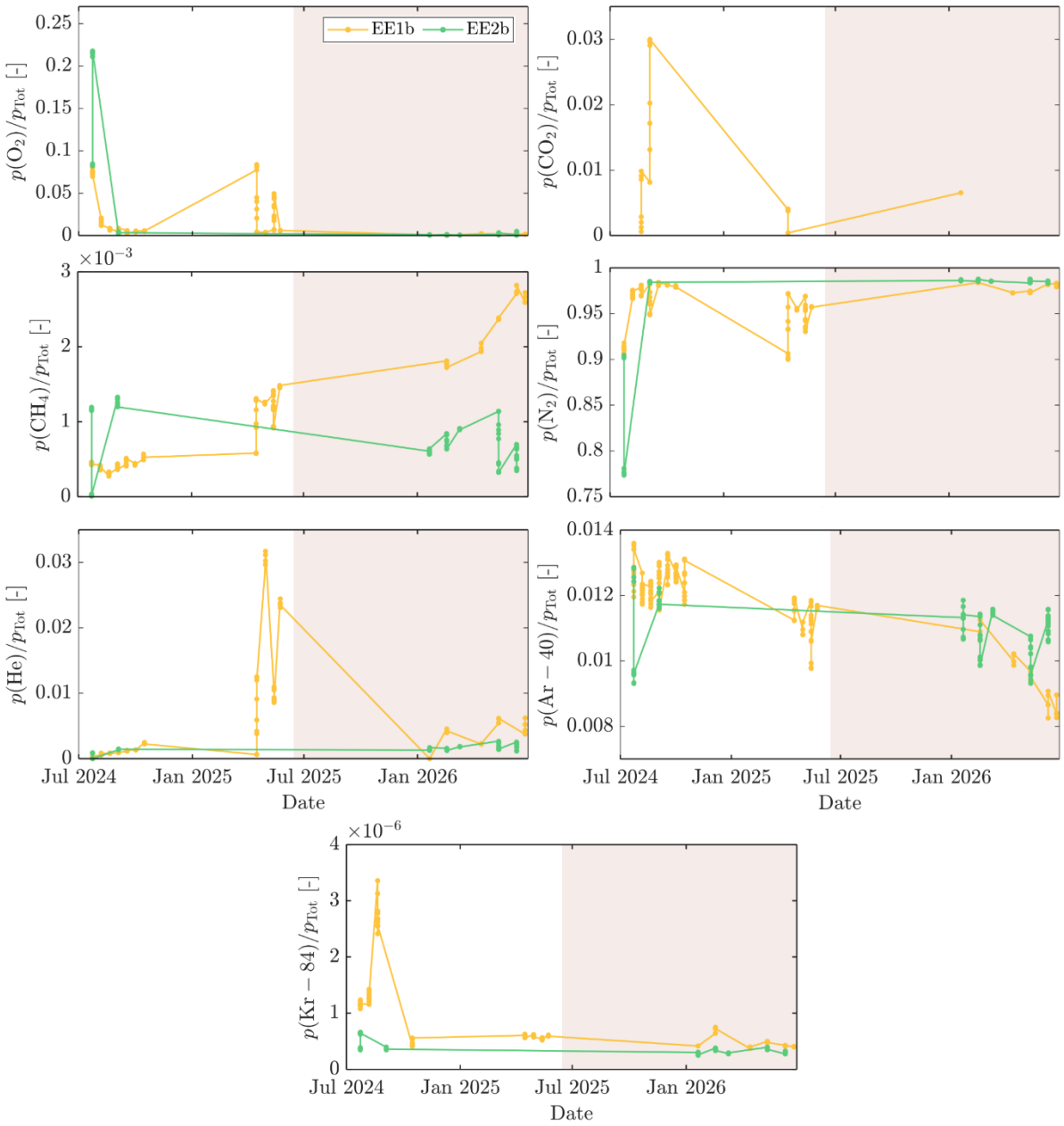

Figure A2. Time series of the concentration of dissolved gases measured in the two sampling locations belonging to the upper freshwater molasse, i.e., EE1b and EE2b. All concentrations, expressed as partial pressures, have been normalized by the total gas pressure, p_{Tot}, measured at each time point. Measured species include dissolved oxygen (O_2), carbon dioxide partial pressure (CO_2), methane (CH_4), dissolved nitrogen (N_2), helium (He), argon-40 (Ar-40), and krypton-84 (Kr-84). The red-hatched area indicates the period since the start of the heat injection.

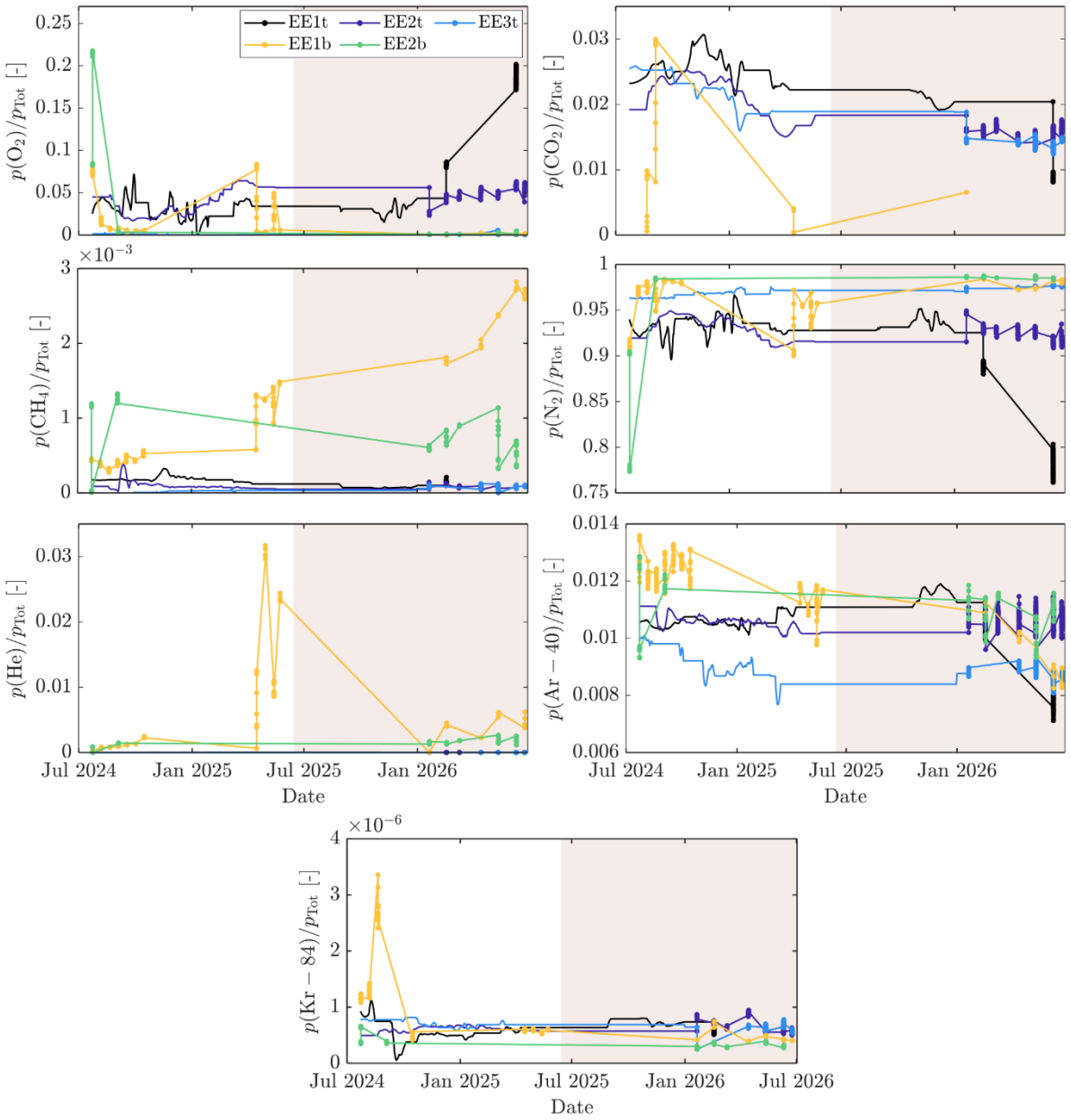

Figure A3. Comparison of the time series of dissolved gases concentration measured both in the top aquifer of low-terrace gravels and glacial-lake deposits and in the upper freshwater molasse. All concentrations, expressed as partial pressures, have been normalized by the total gas pressure, p_{Tot}, measured at each time point. Measured species include dissolved oxygen (O_2), carbon dioxide partial pressure (CO_2), methane (CH_4), dissolved nitrogen (N_2), helium (He), argon-40 (Ar-40), and krypton-84 (Kr-84). The red-hatched area indicates the period since the start of the heat injection.

Appendix 4: Summary of the groundwater chemistry analyses performed for the top aquifer of low-terrace gravels and glacial-lake deposits (EE1t, EE2t, EE3t, and EE4t).

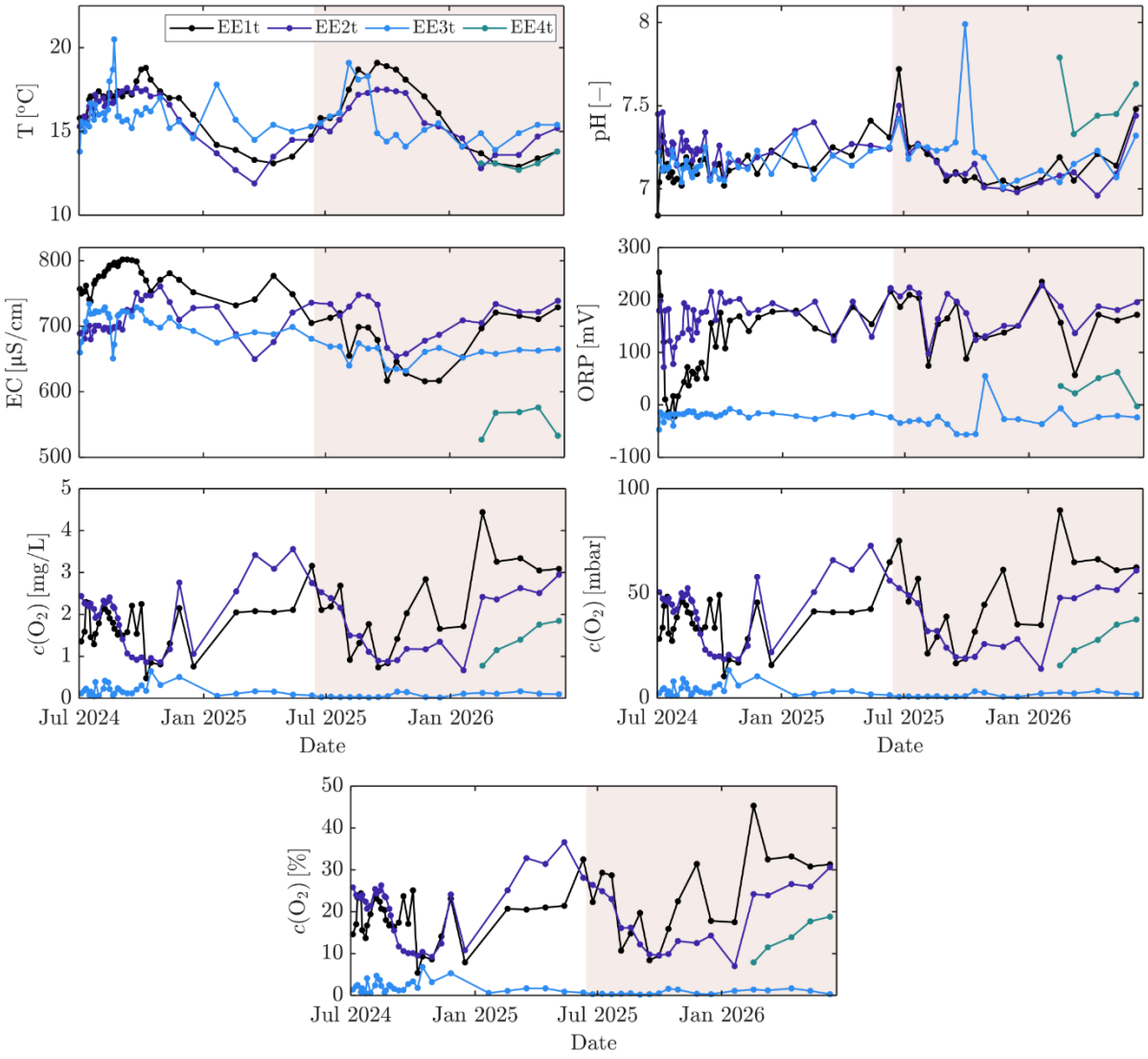

Figure A4. Summary of the groundwater chemistry analyses performed directly on-site during sampling for all sampling locations found in the top aquifer of low-terrace gravels and glacial-lake deposits, i.e., EE1t, EE2t, EE3t, and EE4t. Measured variables include groundwater temperature (T), pH, electrical conductivity (EC), redox potential (ORP), and the concentration of dissolved oxygen (c(O_2)), expressed in units of mg/L, as partial pressure in units of mbar, and as saturation. The red-hatched area indicates the period since the start of the heat injection.

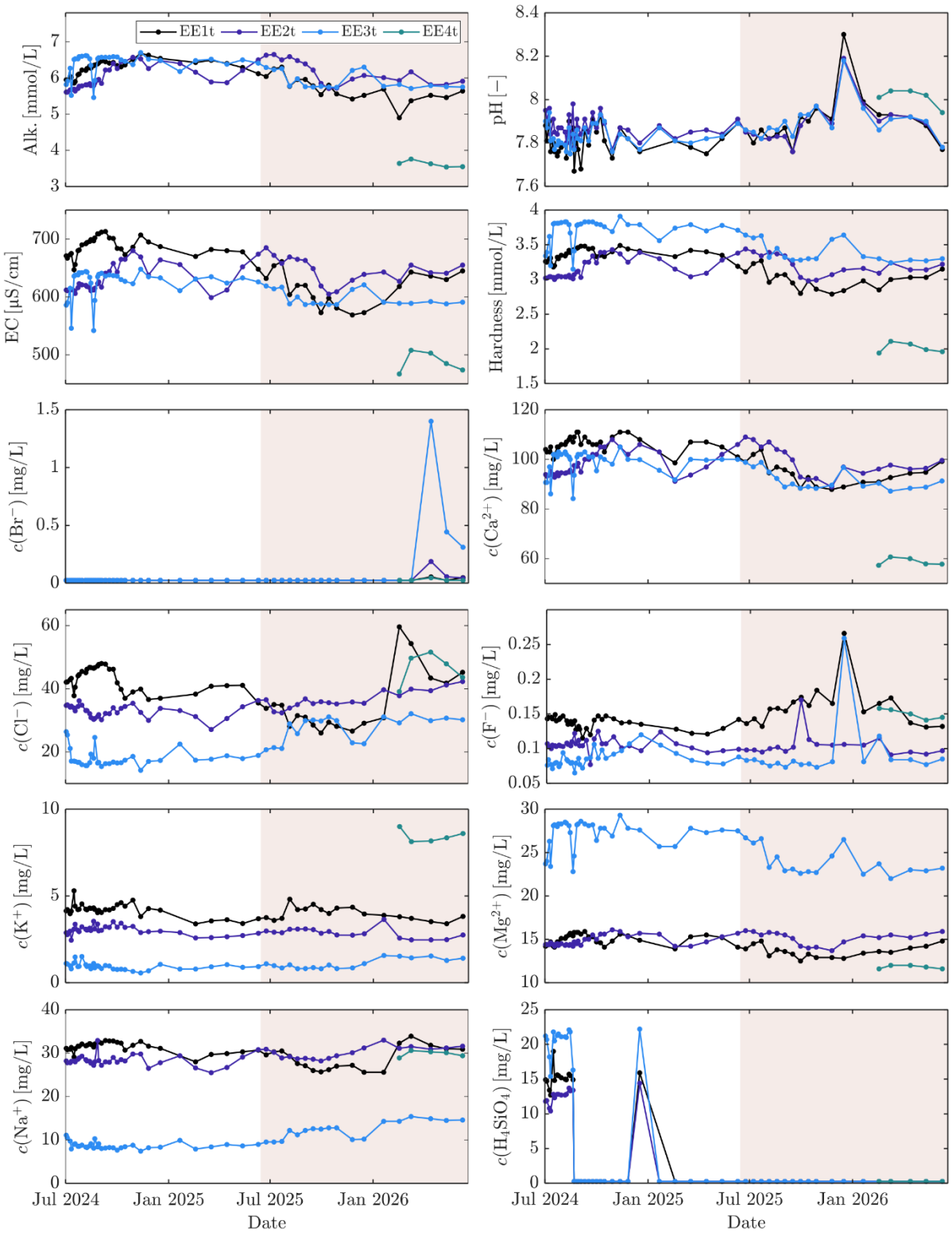

Figure A5. Summary of the time series of some of the properties and compounds measured from laboratory analyses for groundwater chemistry for all sampling locations found in the top aquifer of low-terrace gravels and glacial-lake deposits, i.e., EE1t, EE2t, EE3t, and EE4t. Time series for groundwater properties, such as alkalinity (Alk.), pH, electrical conductivity (EC), and hardness, and for the concentration of some major ions are presented. The red-hatched area indicates the period since the start of the heat injection.

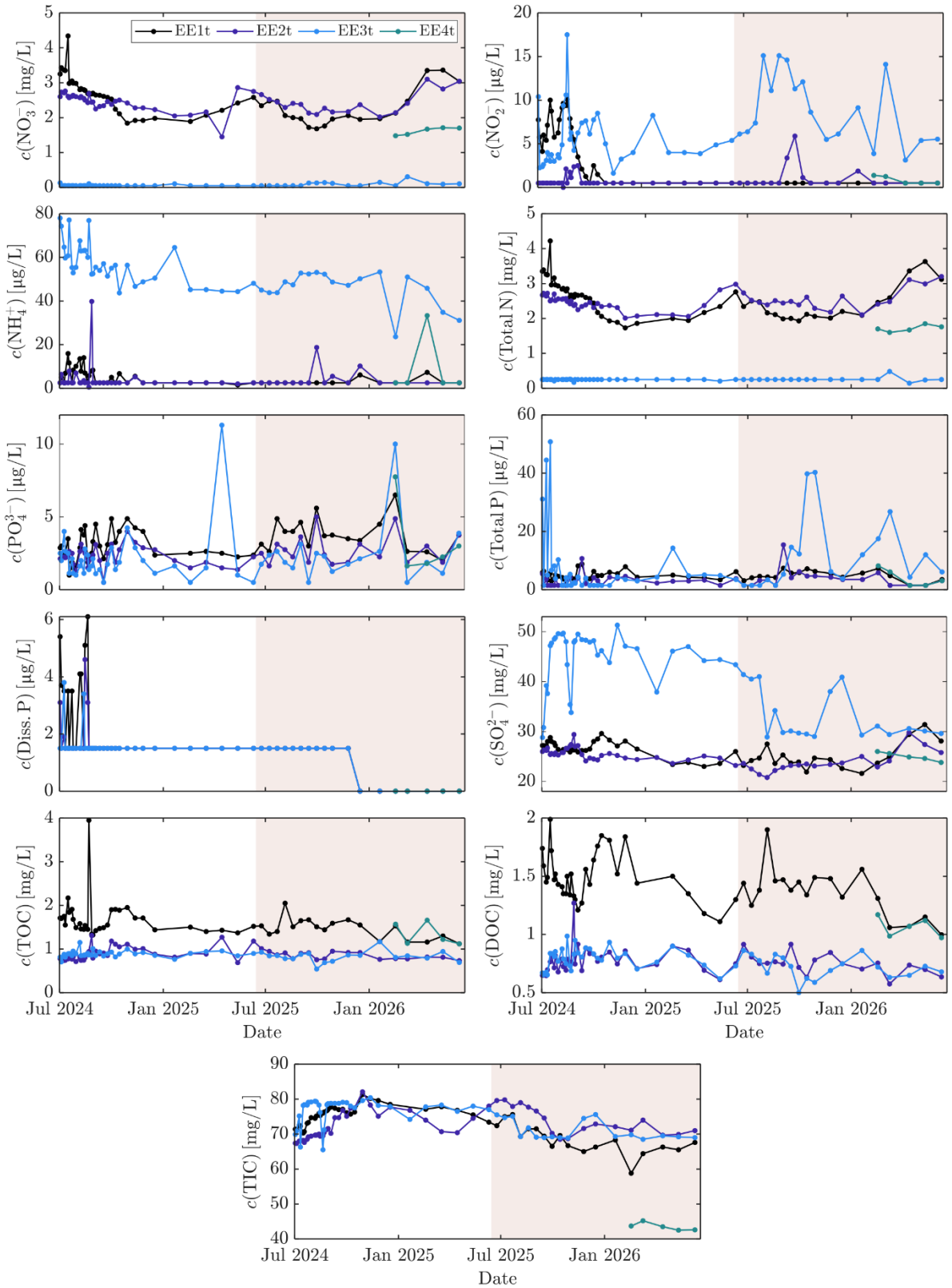

Figure A6. Summary of the time series of some of the variables measured from laboratory analyses for groundwater chemistry for all locations found in the top aquifer of low-terrace gravels and glacial-lake deposits, i.e., EE1t, EE2t, EE3t, and EE4t. They include some macronutrients, such as nitrate (NO_3^-), nitrite (NO_2^-), and ammonium (NH_4^+), total nitrogen, phosphate (PO_4^{3-}), total and dissolved phosphorous, sulfate (SO_4^{2-}), total organic carbon (TOC), dissolved organic carbon (DOC) and total inorganic carbon (TIC). The red-hatched area indicates the period since the start of the heat injection.

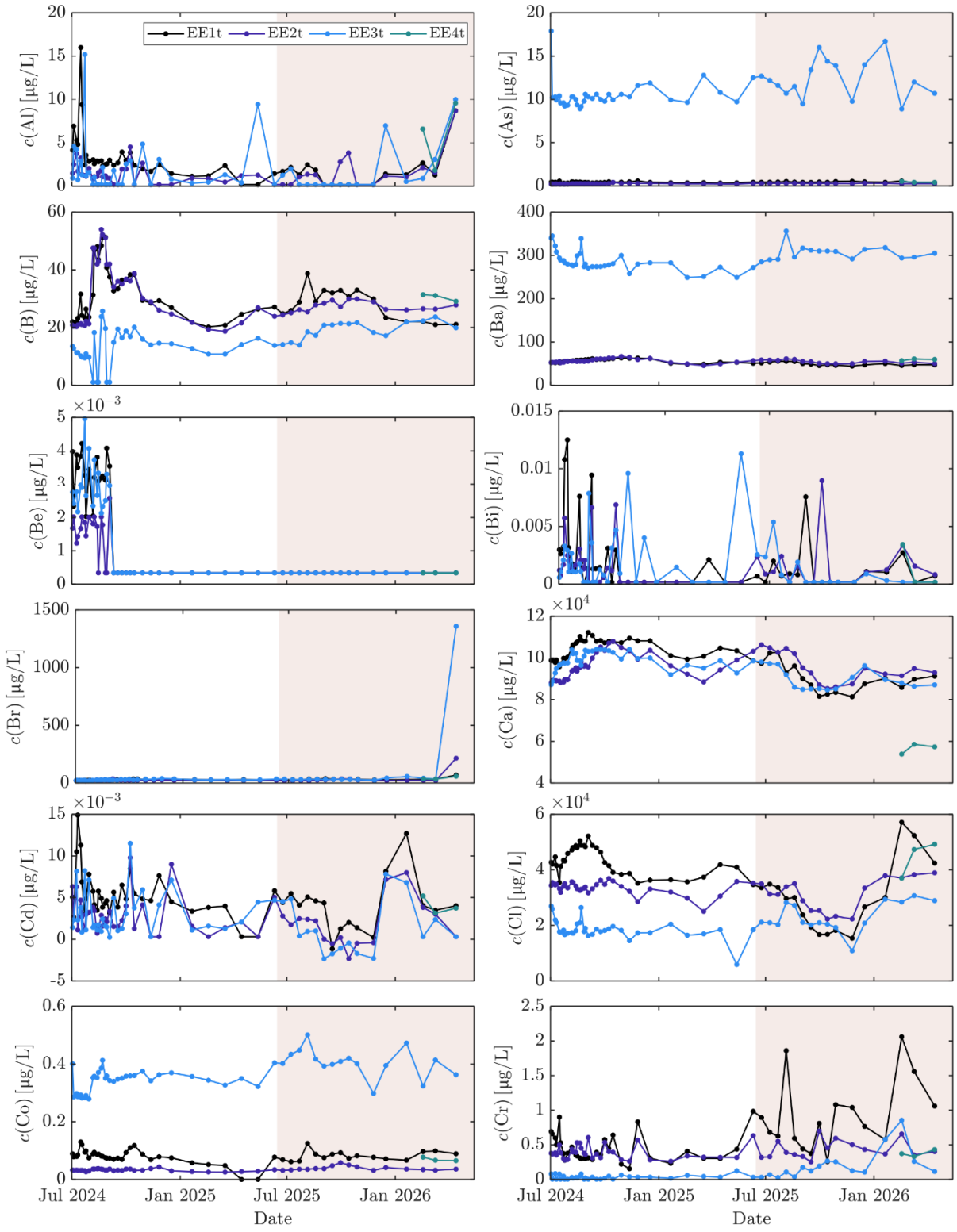

Figure A7. Summary of some of the results obtained from Inductively Coupled Plasma Mass Spectrometry (ICP-MS) on water samples extracted from all sampling locations found in the top aquifer of low-terrace gravels and glacial-lake deposits, i.e., EE1t, EE2t, EE3t, and EE4t. The time series of some of the measured elements are displayed for each sampling location. The red-hatched area indicates the period since the start of the heat injection.

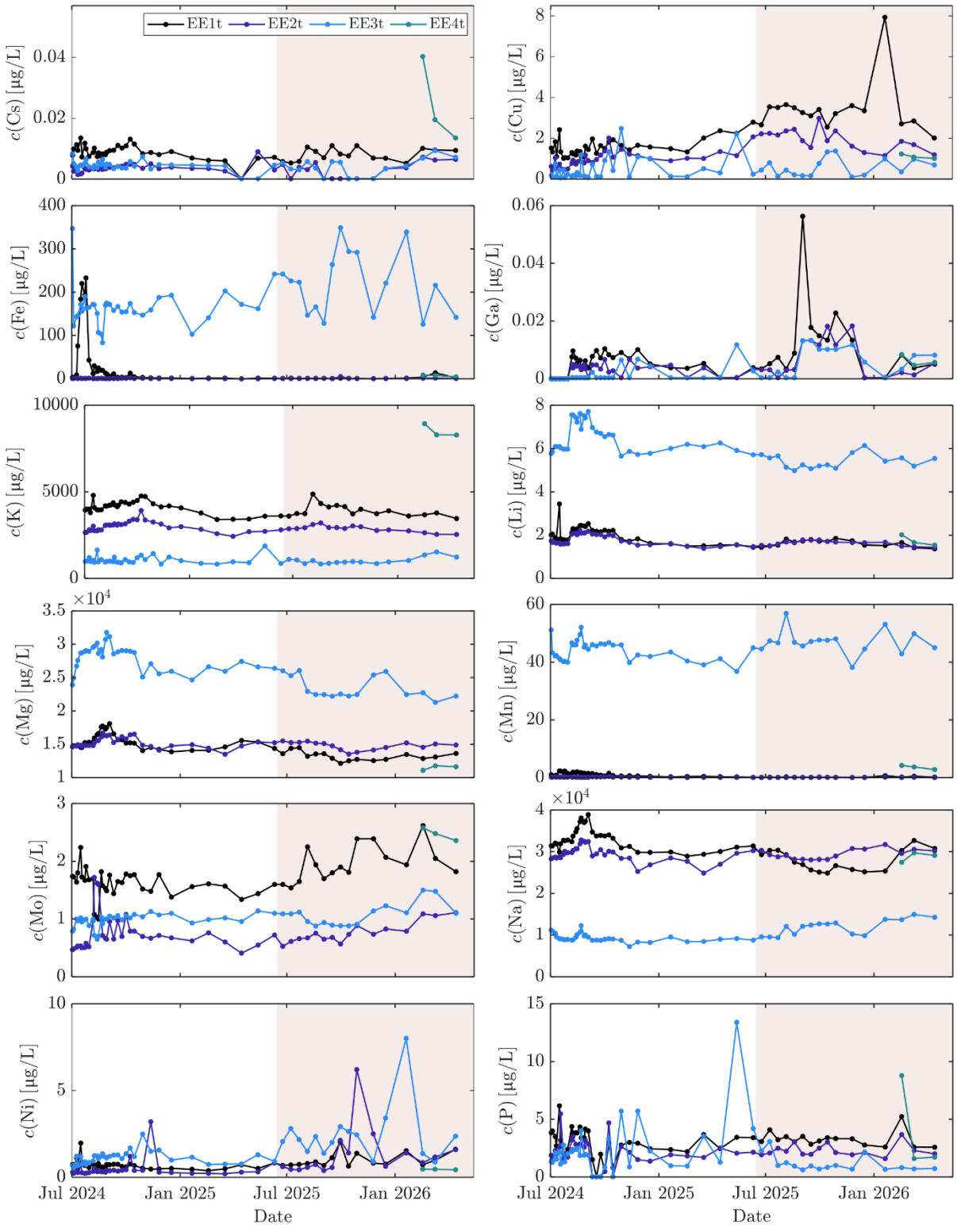

Figure A8. Summary of some of the results obtained from Inductively Coupled Plasma Mass Spectrometry (ICP-MS) on water samples extracted from all sampling locations found in the top aquifer of low-terrace gravels and glacial-lake deposits, i.e., EE1t, EE2t, EE3t, and EE4t. The time series of some of the measured elements are displayed for each sampling location. The red-hatched area indicates the period since the start of the heat injection.

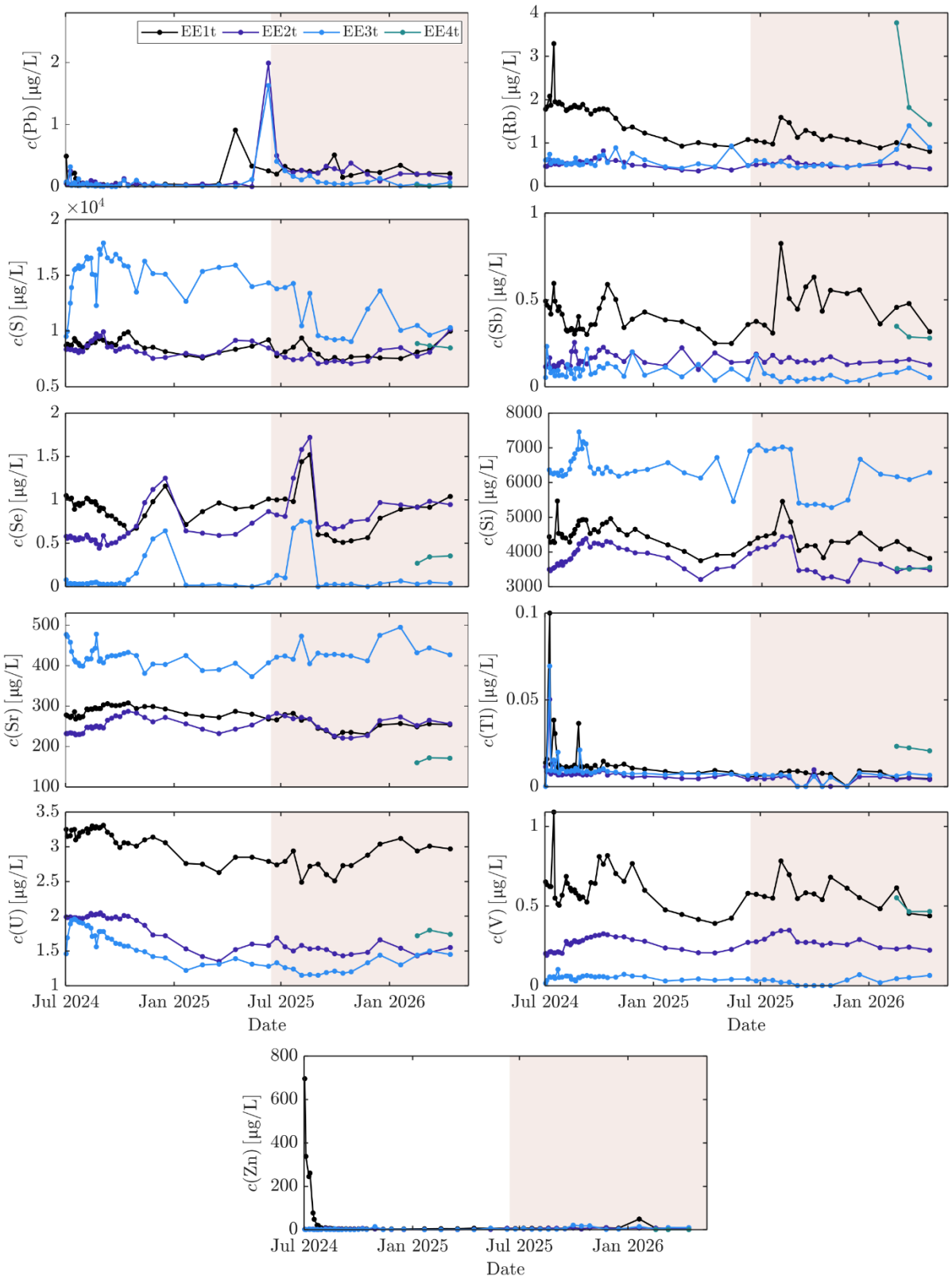

Figure A9. Summary of some of the results obtained from Inductively Coupled Plasma Mass Spectrometry (ICP-MS) on water samples extracted from all sampling locations found in the top aquifer of low-terrace gravels and glacial-lake deposits, i.e., EE1t, EE2t, EE3t, and EE4t. The time series of some of the measured elements are displayed for each sampling location. The red-hatched area indicates the period since the start of the heat injection.

Appendix 5: Summary of the groundwater chemistry analyses performed for the upper freshwater molasse (EE1b and EE2b).

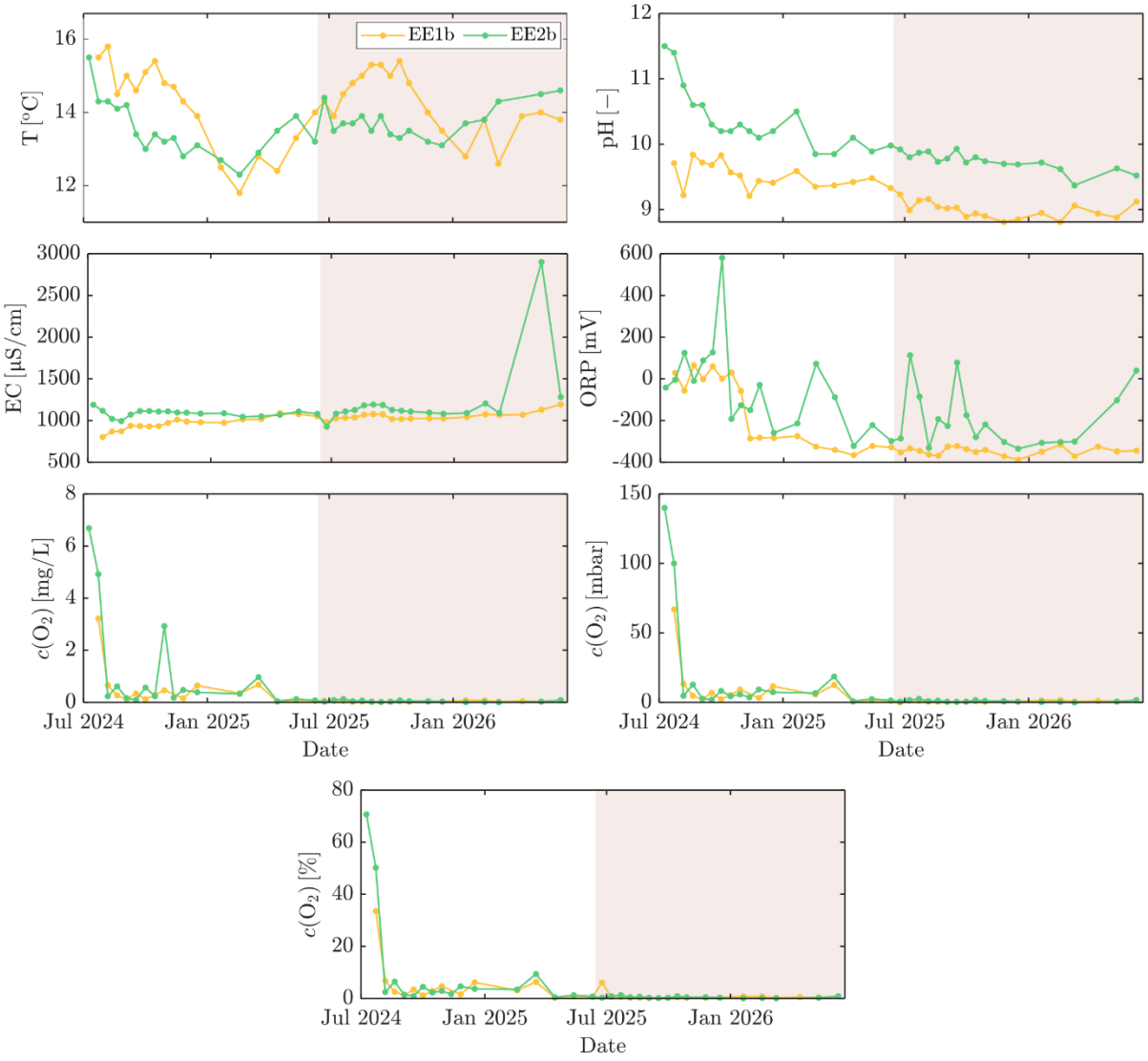

Figure A10. Summary of the groundwater chemistry analyses performed directly on-site during sampling for all sampling locations found in the upper freshwater molasse. Measured variables include groundwater temperature (T), pH, electrical conductivity (EC), redox potential (ORP), and the concentration of dissolved oxygen ($c(O_2)$), expressed in units of mg/L, as partial pressure in units of mbar, and as saturation. The red-hatched area indicates the period since the start of the heat injection.

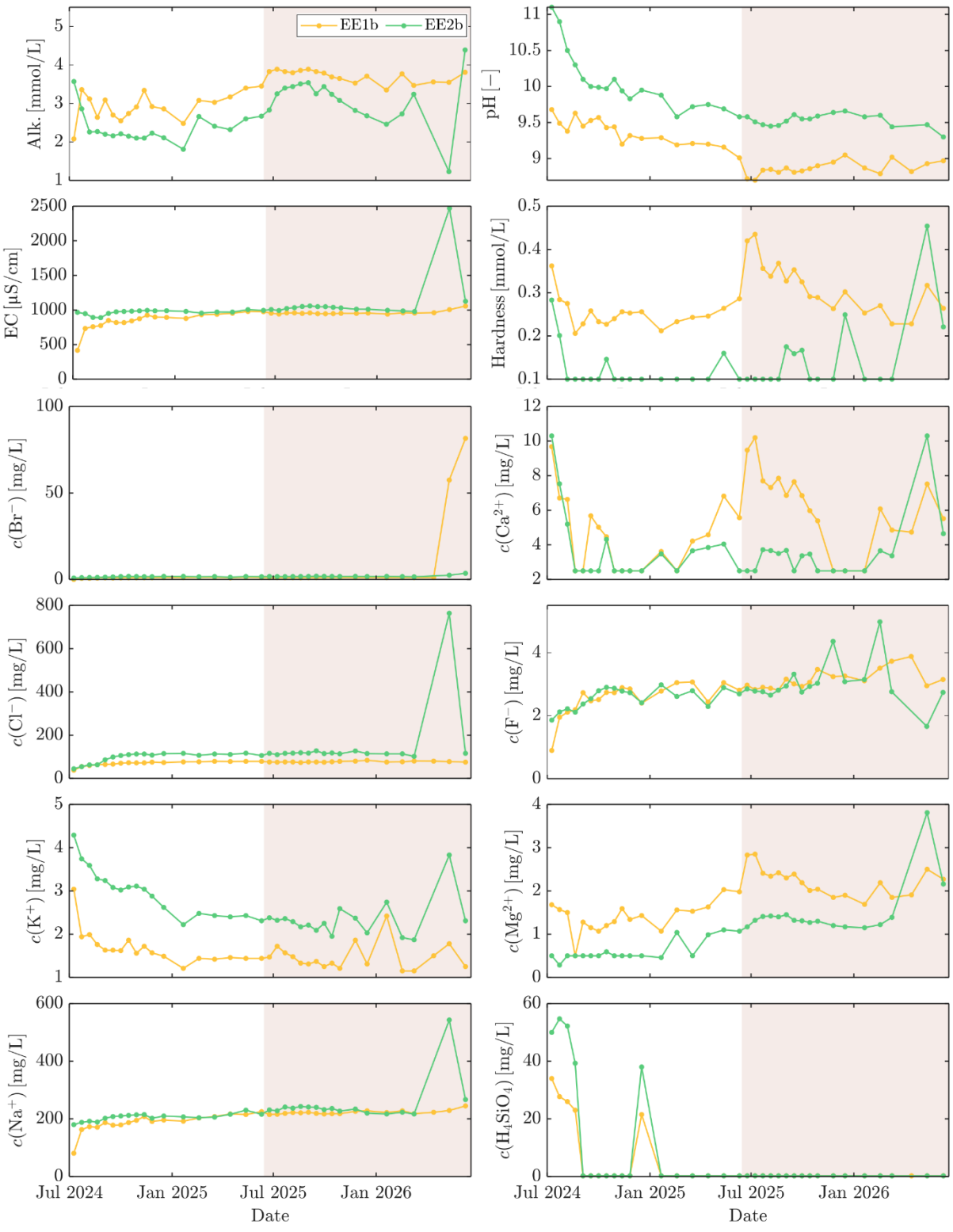

Figure A11. Summary of the time series of some of the properties and compounds measured from laboratory analyses for groundwater chemistry for all locations found in the upper freshwater molasse. Time series for groundwater properties, such as alkalinity (Alk.), pH, electrical conductivity (EC), and hardness, and for the concentration of some major ions are presented. The red-hatched area indicates the period since the start of the heat injection.

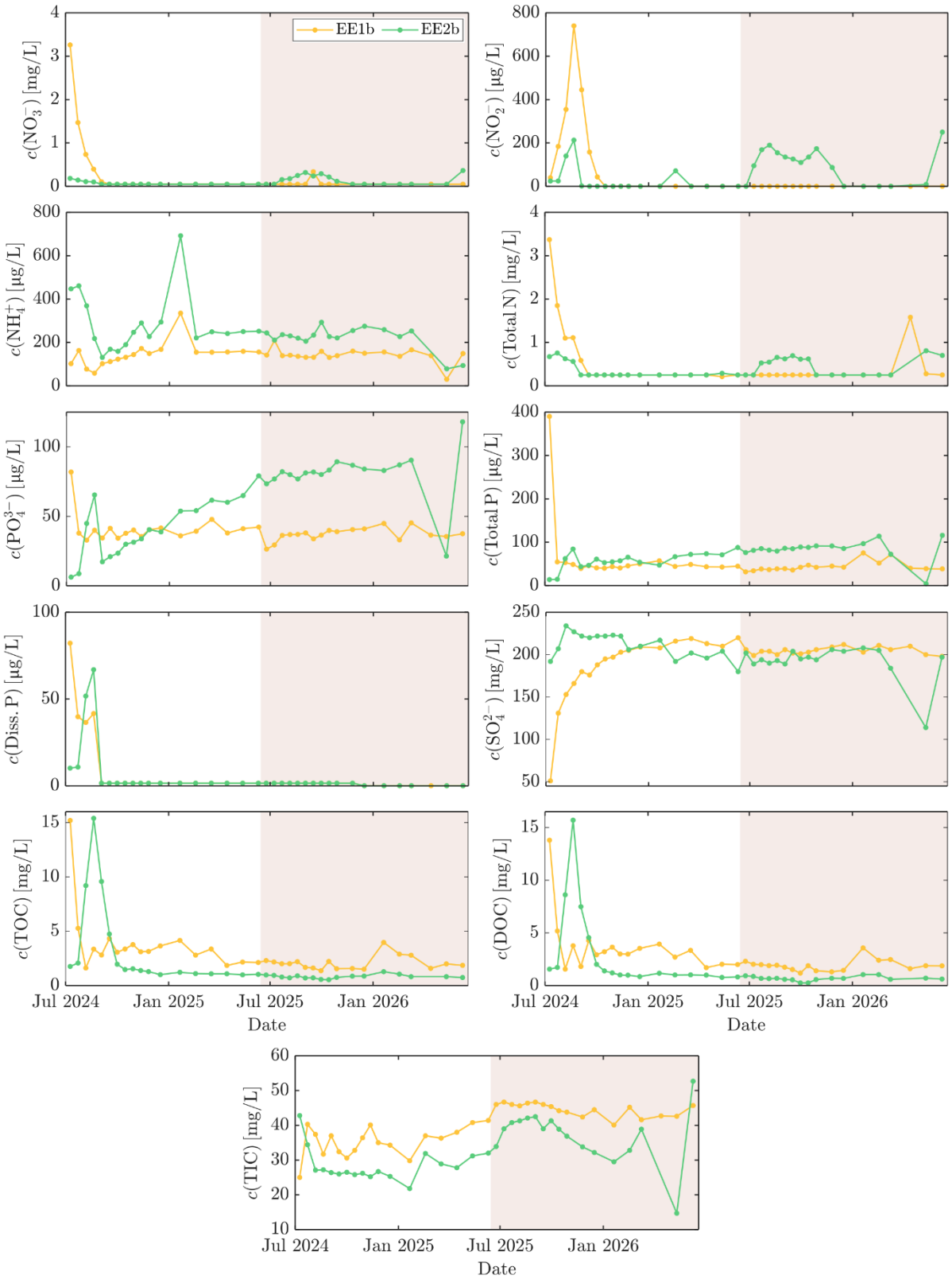

Figure A12. Summary of the time series of some of the variables measured from laboratory analyses for groundwater chemistry for all locations found in the upper freshwater molasse. They include some macronutrients, such as nitrate (NO_3^-), nitrite (NO_2^-), and ammonium (NH_4^+), total nitrogen, phosphate (PO_4^{3-}), total and dissolved phosphorous, sulfate (SO_4^{2-}), total organic carbon (TOC), dissolved organic carbon (DOC) and total inorganic carbon (TIC). The red-hatched area indicates the period since the start of the heat injection.

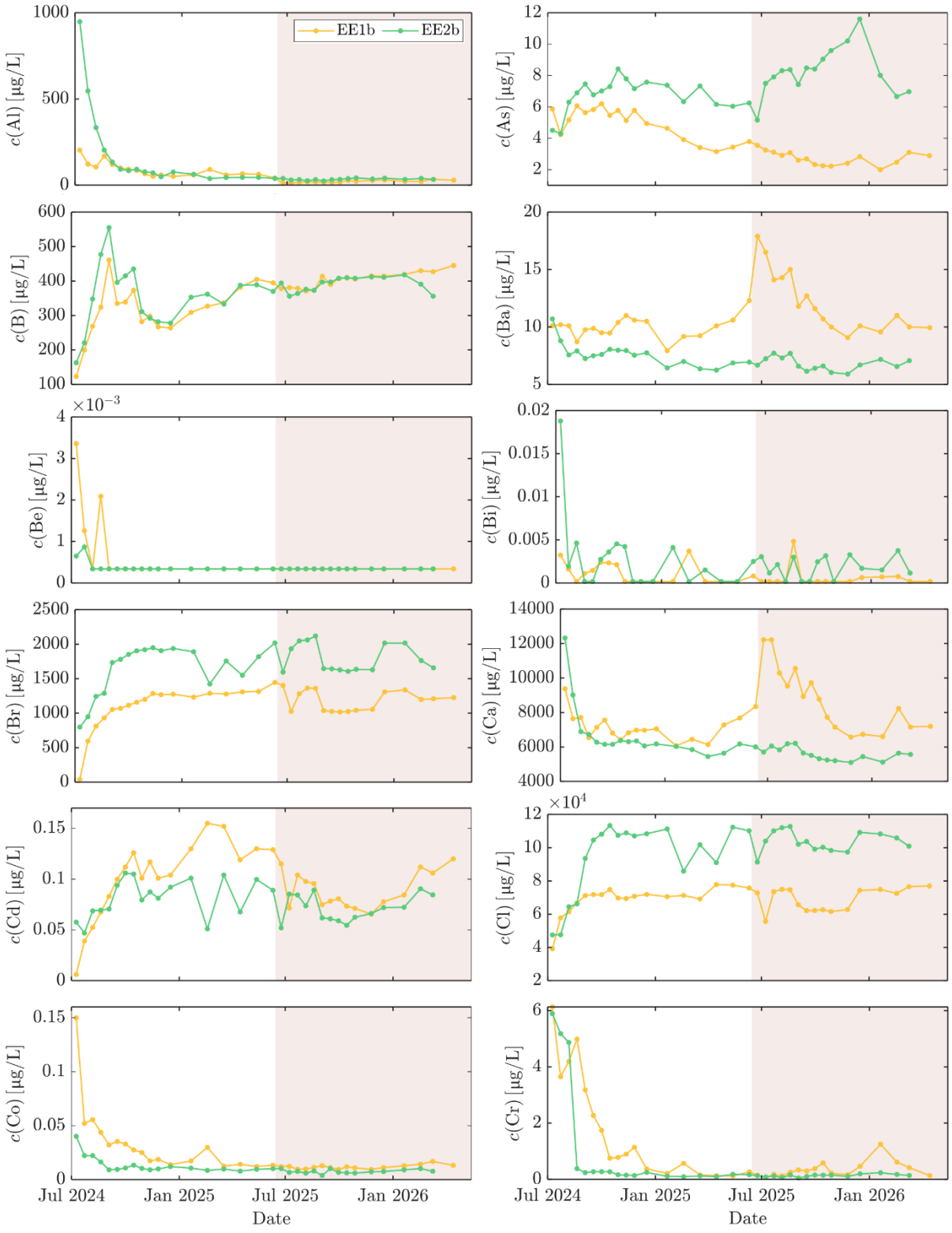

Figure A13. Summary of some of the results obtained from Inductively Coupled Plasma Mass Spectrometry (ICP-MS) on water samples extracted from the upper freshwater molasse. The time series of some of the measured elements are displayed for each sampling location. The red-hatched area indicates the period since the start of the heat injection.

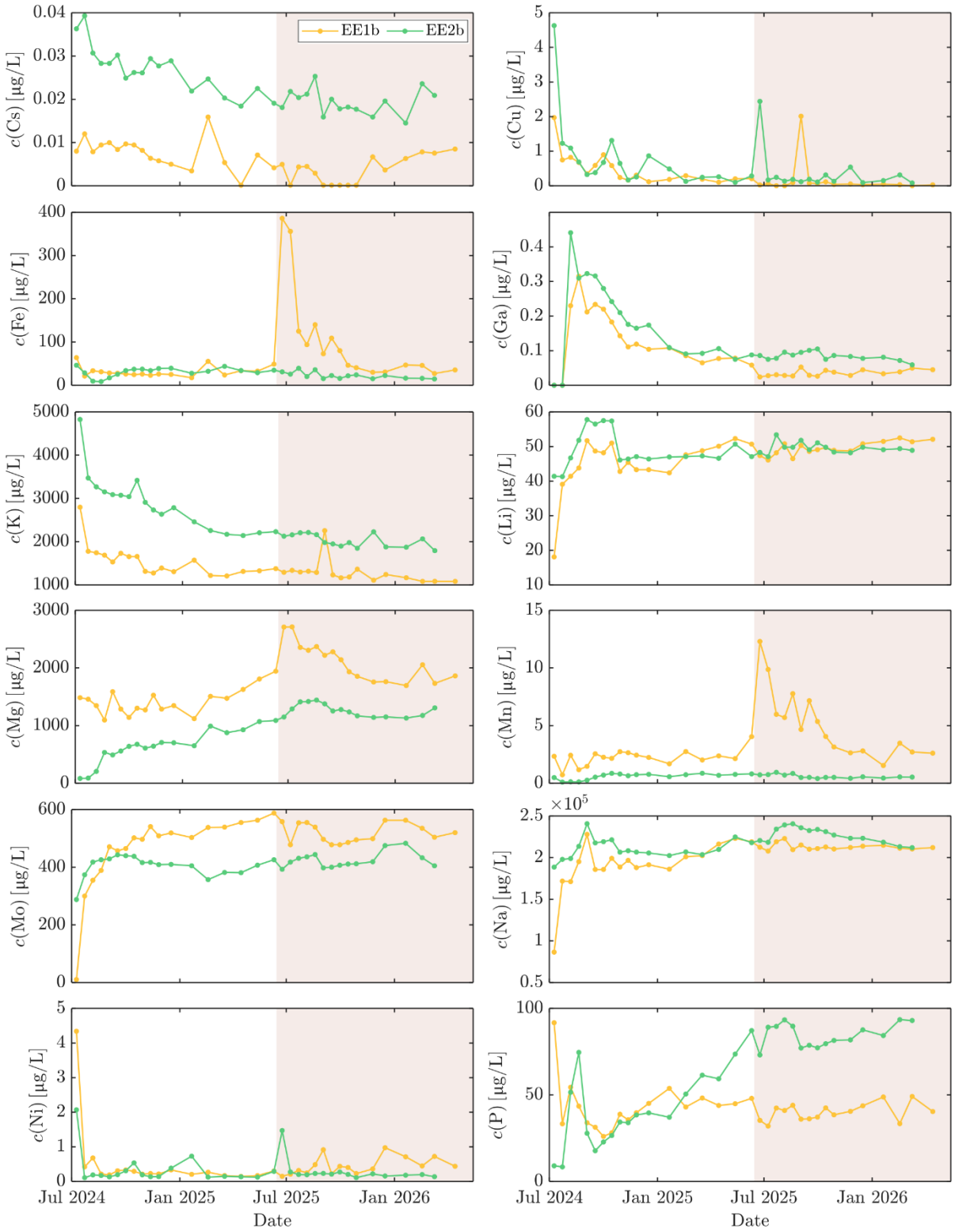

Figure A14. Summary of some of the results obtained from Inductively Coupled Plasma Mass Spectrometry (ICP-MS) on water samples extracted from the upper freshwater molasse. The time series of some of the measured elements are displayed for each sampling location. The red-hatched area indicates the period since the start of the heat injection.

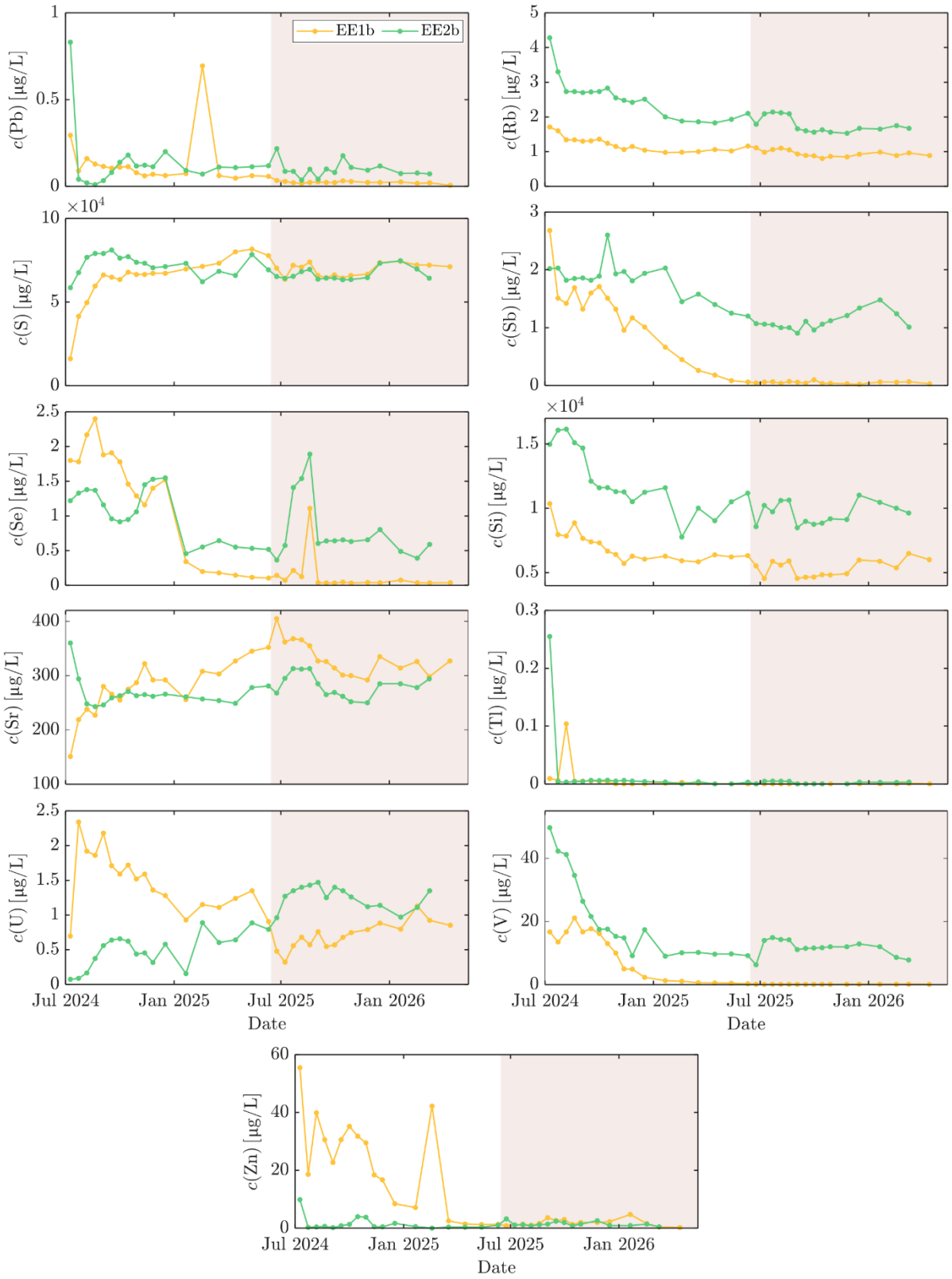

Figure A15. Summary of some of the results obtained from Inductively Coupled Plasma Mass Spectrometry (ICP-MS) on water samples extracted from the upper freshwater molasse. The time series of some of the measured elements are displayed for each sampling location. The red-hatched area indicates the period since the start of the heat injection.